Chapter 2
Conventional SAR imaging

In this chapter, we explain the fundamental principles of SAR data collection and image formation, i.e., inversion of the received data. Synthetic aperture radar uses microwaves for imaging the surface of the Earth from airplanes or satellites. Unlike photography, which generates the picture by essentially recoding the intensity of the light reflected off the different parts of the target, SAR imaging exploits the phase information of the interrogating signals and as such can be categorized as a coherent imaging technology.

To actually obtain the image of an area on the surface of the Earth (the target), a synthetic aperture radar illuminates it with a series of electromagnetic pulses. To do so, the radar antenna is mounted on an airplane or a satellite (called the platform), and the interrogating pulses are emitted by the antenna at different times and locations as it moves along the flight trajectory. Then, the pulses are reflected off the Earth's surface, and the resulting reflected field, which carries the information about the target, is received by the same antenna (monostatic SAR) or a different antenna (bistatic SAR). These received signals represent the raw data. To derive the desired characteristic(s) of the target from the raw data, i.e., to perform the data inversion and create the image, each received signal is first processed by the matched filter. This is a mathematical operation that can be thought of as a certain transformation of the data with the parameters that match those of the received signal in a particular way. Then, the contributions from a series of individual signals are summed up, which amounts to creating a synthetic aperture. This is a key step that creates the image.

The important mathematical concepts associated with SAR imaging include the imaged quantity, the imaging kernel or imaging operator, and the image itself. The imaged quantity is a certain measurable characteristic of the target that we will hereafter interpret as a function $\nu = \nu(\boldsymbol{z})$, where $\boldsymbol{z}$ is the vector of spatial coordinates on the target. In the SAR literature, $\nu(\boldsymbol{z})$ is often referred to as the ground reflectivity function, see, e.g., [86]. The image $I = I(\boldsymbol{y})$ is another function of the spatial coordinates denoted by $\boldsymbol{y}$ in this instance. The relation between the two functions $\nu(\boldsymbol{z})$ and $I(\boldsymbol{y})$ is rendered by the imaging operator.

M. Gilman et al., *Transionospheric Synthetic Aperture Imaging*, Applied and Numerical Harmonic Analysis, DOI 10.1007/978-3-319-52127-5_2

A mathematical theory that describes the formation of SAR images and provides means for their quantitative analysis is known as the SAR ambiguity theory, see [9, 75, 86]. In this theory, the image is represented as a convolution of the ground reflectivity $\nu(\boldsymbol{z})$ with the imaging kernel $W(\boldsymbol{y}, \boldsymbol{z}) = W(\boldsymbol{y} - \boldsymbol{z})$ that characterizes the radar system:

$$I(\boldsymbol{y}) = \int \nu(\boldsymbol{z}) W(\boldsymbol{y}, \boldsymbol{z}) d\boldsymbol{z}. \tag{2.1}$$

Formula (2.1) defines the imaging operator as linear. It allows for a rigorous mathematical analysis of the image properties, in particular, its resolution, i.e., the capability to distinguish between the closely located point targets. Indeed, in the ideal case, where $W(\boldsymbol{y}, \boldsymbol{z}) = \delta(\boldsymbol{y} - \boldsymbol{z})$, the imaging operator becomes an identity and the image $I(\boldsymbol{y})$ coincides with the unknown ground reflectivity $\nu(\boldsymbol{z})$. In more realistic situations though, the kernel $W(\boldsymbol{y}, \boldsymbol{z})$, which is often referred to as the generalized ambiguity function (GAF), is never equal to the δ-function. Hence, the imperfections of the image can be unambiguously attributed to the properties of the kernel and as such, to those of the imaging system.

In the rest of this chapter we will derive and analyze the expression for the imaging kernel $W(\boldsymbol{y}, \boldsymbol{z})$ and justify formula (2.1). Representation (2.1) will allow us to see, in particular, how the parameters of the imaging system affect the final quality of the image, because those parameters get incorporated into the kernel $W(\boldsymbol{y}, \boldsymbol{z})$. They include the carrier frequency, the shape and repetition frequency of the interrogating pulses, the shape of the flight trajectory, as well as the direction and shape of the propagating radar beam that are partially determined by the characteristics of the antenna.

For the analysis in this chapter, we will employ the start-stop approximation that considers the antenna motionless when each interrogating pulse is emitted and the scattered response is received, after which the antenna moves to the next sending/receiving position along its trajectory. The analysis of the start-stop approximation is provided in Chapter 6. The additional assumptions that we make in this chapter include:

- The interrogating field is considered scalar and no polarization is taken into account. The discussion that involves the actual vector electromagnetic fields and their polarization is deferred until Chapters 5, 7, and 8. In this chapter, the scalar interrogating field can be thought of as a given component of the true vector electric field.
- The platform trajectory is taken as a straight line, which is good approximation for a short stretch of the satellite orbit. The direction of the antenna beam has a fixed angle with respect to the flight direction, which means that the beam footprint sweeps a strip, or swath, on the Earth's surface parallel to the orbit as the antenna moves. Once combined with the processing by means of a matched filter, this scenario is known as the stripmap SAR imaging. If, in addition, the direction of the beam is normal to the platform trajectory, then we have a broadside stripmap imaging.

- The scattering of radar signals off the target is linearized via the first Born approximation. The deficiencies of this approach are outlined in Section 2.7. The remedy is proposed in Chapter 7.
- The target is thought of as deterministic and dispersionless. In reality, dispersion of the target may be very significant, and we identify its analysis in the context of transionospheric SAR imaging as one of the important directions for future study, see Chapter 9.
- Only standard non-interferometric SAR imaging is considered. The properties of the imaged terrain may vary along the flight trajectory (the azimuthal direction) and across the flight trajectory (the range direction). No terrain elevation is taken into account.

These assumptions will be delineated on as the exposition of the material unfolds. Other assumptions will be introduced and explained as needed.

2.1 Propagation and scattering of radar signals

In the framework of the conventional SAR ambiguity theory, see [9, 75, 86], the radar signals are interpreted as scalar quantities. Their propagation in free space is governed by the d'Alembert (or wave) equation:

$$\Big(\frac{1}{c^2}\frac{\partial^2}{\partial t^2} - \Delta\Big)u = f, \tag{2.2}$$

where Δ is the Laplacian, c is the speed of light, and $f = f(t, \boldsymbol{z})$ is the density of the sources, $\boldsymbol{z} \in \mathbb{R}^3$.

For an unsteady point source (the emitting radar antenna) located at a fixed $\boldsymbol{x} \in \mathbb{R}^3$, the density is defined as

$$f(t, \boldsymbol{z}) = P(t)\delta(\boldsymbol{z} - \boldsymbol{x}), \tag{2.3}$$

and the solution of equation (2.2) written as the Kirchhoff integral reduces to the standard retarded potential:

$$\begin{aligned} u^{(0)}(t, \boldsymbol{z}) &= \frac{1}{4\pi}\iiint\limits_{\mathbb{R}^3} \frac{f(t - |\boldsymbol{z} - \boldsymbol{z}'|/c, \boldsymbol{z}')}{|\boldsymbol{z} - \boldsymbol{z}'|} d\boldsymbol{z}' \\ &= \frac{1}{4\pi}\iiint\limits_{\mathbb{R}^3} \frac{\delta(\boldsymbol{z}' - \boldsymbol{x})}{|\boldsymbol{z} - \boldsymbol{z}'|} P\Big(t - \frac{|\boldsymbol{z} - \boldsymbol{z}'|}{c}\Big) d\boldsymbol{z}' \\ &= \frac{1}{4\pi}\frac{P(t - |\boldsymbol{z} - \boldsymbol{x}|/c)}{|\boldsymbol{z} - \boldsymbol{x}|}. \end{aligned} \tag{2.4}$$

Note that the integration over the entire $\mathbb{R}^3$ in formula (2.4) corresponds to formally considering $t > -\infty$, as opposed to the more traditional choice $t \geq 0$ (that would also require specifying the initial conditions). Hereafter, solution (2.4) will be used in the capacity of the incident field.

Suppose that the terrain to be imaged is characterized by the refractive index $n = n(\boldsymbol{z})$. Then, the total field $u = u^{(0)} + u^{(1)}$ is governed by the variable coefficient wave equation:

$$\Big(\frac{1}{v^2(\boldsymbol{z})}\frac{\partial^2}{\partial t^2} - \Delta\Big)\big(u^{(0)} + u^{(1)}\big) = f, \tag{2.5}$$

where $u^{(1)} = u^{(1)}(t, \boldsymbol{z})$ is the scattered field and $v(\boldsymbol{z}) = \frac{c}{n(\boldsymbol{z})}$ is the speed of light in the material. In the vacuum region, it is assumed that $n(\boldsymbol{z}) = 1$ so that $v(\boldsymbol{z}) = c$ and equation (2.5) transforms back to (2.2). Subtracting the constant coefficient equation (2.2) written for the incident field $u^{(0)}$ on the entire space $\mathbb{R}^3$ from the variable coefficient equation (2.5), we have:

$$\Big(\frac{1}{c^2}\frac{\partial^2}{\partial t^2} - \Delta\Big)u^{(1)} = \frac{1 - n^2(\boldsymbol{z})}{c^2}\frac{\partial^2}{\partial t^2}\big(u^{(0)} + u^{(1)}\big). \tag{2.6}$$

Equation (2.6) involves no simplifying assumptions, and its solution $u^{(1)}$ is the same as one would have obtained by solving (2.5) with $u^{(0)}$ found from (2.2). Hence, this linear variable coefficient partial differential equation can be used for direct computation of the scattered field $u^{(1)}$ if the incident field $u^{(0)}$ and the refractive index $n(\boldsymbol{z})$ are given.

However, the central problem of SAR imaging is rather the inverse problem of reconstructing the unknown material parameter $n(\boldsymbol{z})$, given the incident field $u^{(0)}$ and taking the scattered field $u^{(1)}$ as the observable data. In that regard, it is very important to realize that whereas the incident field $u^{(0)}$ is known on the entire $\mathbb{R}^3$, the scattered field $u^{(1)}$ can be considered known only at certain locations away from the target region.[1] Thus, the inverse problem of SAR imaging becomes effectively nonlinear, because on the right-hand side of equation (2.6) the unknown quantity of interest $n(\boldsymbol{z})$ is multiplied by another unknown quantity, $u^{(1)}(t, \boldsymbol{z})$.

2.1.1 The first Born approximation

The most common assumption made in the SAR literature in order to simplify the formulation of the inverse problem is that of weak scattering:

$$|n(\boldsymbol{z}) - 1| \ll 1, \quad |u^{(1)}| \ll |u^{(0)}|. \tag{2.7}$$

[1] In practice, $u^{(1)}$ is known at the receiving radar antenna, which is mounted on an airborne or spaceborne platform located above the imaged terrain (Earth's surface), see Figure 2.1.

Relations (2.7) allow one to employ the first Born approximation [107, Section 13.1.2] and linearize equation (2.6) by disregarding $u^{(1)}$ on its right-hand side. This linearization yields an inhomogeneous d'Alembert equation for the scattered field:

$$\Big(\frac{1}{c^2}\frac{\partial^2}{\partial t^2} - \Delta\Big)u^{(1)} = \frac{1-n^2(\boldsymbol{z})}{c^2}\frac{\partial^2 u^{(0)}}{\partial t^2}. \tag{2.8}$$

The source term on the right-hand side of (2.8) is due to the incident field $u^{(0)}(t, \boldsymbol{z})$ of (2.4) and variable refractive index $n(\boldsymbol{z})$. The solution to equation (2.8) is given by the Kirchhoff integral:

$$u^{(1)}(t, \boldsymbol{x}') = \frac{1}{4\pi}\int \frac{1-n^2(\boldsymbol{z})}{|\boldsymbol{x}'-\boldsymbol{z}|c^2}\frac{\partial^2 u^{(0)}}{\partial t^2}\big(t-|\boldsymbol{x}'-\boldsymbol{z}|/c, \boldsymbol{z}\big)\,d\boldsymbol{z}, \tag{2.9}$$

where $\boldsymbol{x}'$ can be an arbitrary point in $\mathbb{R}^3$. One can think of $\boldsymbol{x}'$ as the location of the receiving antenna. For monostatic SAR, it coincides with that of the emitting antenna, $\boldsymbol{x}' = \boldsymbol{x}$.

Hereafter, we will consider the emitted signal in the form of a linear frequency-modulated pulse, or chirp, with the central carrier frequency ω_0:

$$P(t) = A(t)e^{-i\omega_0 t}, \quad \text{where} \quad A(t) = \chi_\tau(t)e^{-i\alpha t^2} \tag{2.10}$$

and χ_τ is the indicator function:

$$\chi_\tau(t) = \begin{cases} 1, & t \in [-\tau/2, \tau/2], \\ 0, & \text{otherwise.} \end{cases} \tag{2.11}$$

In formula (2.10), $\alpha = \frac{B}{2\tau}$ is the chirp rate, $\frac{B}{2\pi}$ is called the bandwidth of the chirp, and τ is its duration. The time-bandwidth product (TBP) of the chirp, $\frac{B\tau}{2\pi}$, also known as its compression ratio (see Section 2.6), is assumed large: $B\tau \gg 1$.[2] As the indicator χ_τ of (2.11) is compactly supported on $[-\tau/2, \tau/2]$, the chirp can be approximately thought of as a band limited function. Indeed, its instantaneous frequency (as defined, e.g., in [86, Section 5.2.1] via a stationary phase argument)

$$\omega(t) \stackrel{\text{def}}{=} \frac{d}{dt}(\omega_0 t + \alpha t^2) = \omega_0 + 2\alpha t = \omega_0 + \frac{B}{\tau}t \tag{2.12}$$

varies between $\omega_0 - B/2$ and $\omega_0 + B/2$. The true spectrum of the chirp, of course, is not confined to the interval $[\omega_0 - B/2, \omega_0 + B/2]$ (see Appendix 2.A and specifically footnote[9] on page 57, as well as Section 3.2, page 75, for additional detail.)

[2] In Section 2.6, we will see that a large value of $B\tau$ is what enables the SAR resolution in range.

Nonetheless, B is commonly interpreted as the frequency band of the chirp. For typical SAR applications it is assumed narrow: $B \ll \omega_0$. This implies that the amplitude $A(t)$ in (2.10) varies slowly compared to the fast carrier oscillation $e^{-i\omega_0 t}$, because $|\alpha\tau| \ll \omega_0$. Hence, $A(t)$ can be left out when differentiating the incident field (2.4) for substitution into (2.8), which yields:

$$\frac{\partial^2 u^{(0)}}{\partial t^2}(t, \boldsymbol{z}) \approx -\omega_0^2 u^{(0)}(t, \boldsymbol{z}) = -\frac{\omega_0^2}{4\pi} \frac{P(t - |\boldsymbol{z} - \boldsymbol{x}|/c)}{|\boldsymbol{z} - \boldsymbol{x}|}. \tag{2.13}$$

Consequently, from equation (2.9) we have:

$$u^{(1)}(t, \boldsymbol{x}') \approx \int \nu(\boldsymbol{z}, \boldsymbol{x}, \boldsymbol{x}') P\left(t - |\boldsymbol{x} - \boldsymbol{z}|/c - |\boldsymbol{x}' - \boldsymbol{z}|/c\right) d\boldsymbol{z}, \tag{2.14}$$

where

$$\nu(\boldsymbol{z}, \boldsymbol{x}, \boldsymbol{x}') = -\frac{\omega_0^2}{16\pi^2 |\boldsymbol{z} - \boldsymbol{x}||\boldsymbol{z} - \boldsymbol{x}'|} \frac{1 - n^2(\boldsymbol{z})}{c^2}. \tag{2.15}$$

For common SAR geometries, the distance between either of the antennas, $\boldsymbol{x}$ or $\boldsymbol{x}'$, and the target is much larger than the resolution scale at the target, which can be considered a typical variation of $\boldsymbol{z}$. A schematic for the monostatic broadside imaging ($\boldsymbol{x} = \boldsymbol{x}'$) is shown in Figure 2.1. Moreover, this distance is also much larger than the typical variation of either $\boldsymbol{x}$ or $\boldsymbol{x}'$, which is characterized by the length of the synthetic aperture introduced in Section 2.3.2. Hence, given that the quantity $1 - n^2(\boldsymbol{z})$ on the right-hand side of (2.15) is already small due to the first relation of (2.7), one can disregard the dependence of the denominator in formula (2.15) on any of the variables $\boldsymbol{z}$, $\boldsymbol{x}$, or $\boldsymbol{x}'$, i.e., interpret it as a constant. Indeed, taking the variation of the denominator into account would bring along a correction proportional to the product of two small terms, which does not need to be considered in the context of the Born linearization.

Consequently, we can replace equations (2.14) and (2.15) with

$$u^{(1)}(t, \boldsymbol{x}') \approx \int \nu(\boldsymbol{z}) P\left(t - |\boldsymbol{x} - \boldsymbol{z}|/c - |\boldsymbol{x}' - \boldsymbol{z}|/c\right) d\boldsymbol{z}, \tag{2.14$'$}$$

and

$$\nu(\boldsymbol{z}) = -\frac{\omega_0^2}{16\pi^2 R^2} \frac{1 - n^2(\boldsymbol{z})}{c^2}, \tag{2.15$'$}$$

respectively, where R is the distance (slant range) between the SAR platform trajectory (e.g., satellite orbit) and the target,[3] see Figure 2.1. The ground reflectivity function $\nu(\boldsymbol{z})$ in (2.14$'$), (2.15$'$) therefore becomes a function of the local index of refraction $n(\boldsymbol{z})$ only.

[3] We are assuming in (2.15$'$) that this distance is the same for both antennas, $\boldsymbol{x}$ and $\boldsymbol{x}'$.

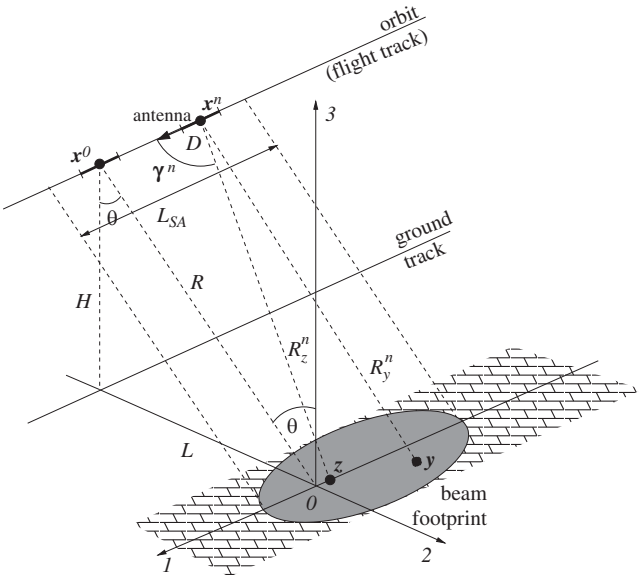

Fig. 2.1 Schematic for the monostatic broadside stripmap SAR imaging. H is the orbit altitude, L is the distance (range) from the ground track to the target, R is the slant range, θ is the angle of incidence or the look angle, and D is the length of a linear antenna. (This figure is a modified version of [7, Figure 1]. Copyright ©2015 Society for Industrial and Applied Mathematics. Reprinted with permission. All rights reserved. Two different earlier versions have also appeared as [5, Figure 1] and [6, Figure 1]. Copyright ©2013, 2014 IOP Publishing. Reproduced with permission. All rights reserved.)

Next, we will discuss how the foregoing linearized model based on weak scattering can be used for the analysis of SAR imaging. In doing so, we will consider only the case of a monostatic SAR, i.e., $\boldsymbol{x}' = \boldsymbol{x}$. Then, equation (2.14′) becomes

$$u^{(1)}(t, \boldsymbol{x}) \approx \int v(\boldsymbol{z}) P\left(t - 2|\boldsymbol{x} - \boldsymbol{z}|/c\right) d\boldsymbol{z}. \tag{2.14″}$$

Our goal is to perform the inversion, i.e., find the unknown $v(\boldsymbol{z})$ while interpreting $u^{(1)}(t, \boldsymbol{x})$ as given data. To do so, we first need to describe the geometry of the propagation of radar signals.

Hereafter, we will be using the Cartesian coordinates labeled by subscripts as follows: "1" will correspond to the azimuthal, or along-the-track, coordinate, "2" will correspond to the range coordinate, i.e., the horizontal coordinate normal to the track, and "3" will correspond to the vertical coordinate. For convenience, and with no loss of generality, we place the origin of the coordinate system in the target area on the ground (rather than directly underneath the platform, i.e., on the ground track). In addition, we denote by θ the angle of incidence, which in our case also coincides with the look angle or elevation angle, because we do not take into account the curvature of the Earth's surface. Then, the orbit altitude becomes $H = R\cos\theta$ and the distance from the origin to the ground track is given by $L = R\sin\theta$, see Figure 2.1.

2.2 Radiation pattern of the antenna

To begin with, we note that the standard retarded potential (2.4) represents the radiation of waves by a stationary point source. It can be used for describing the SAR pulses because we are employing the start-stop approximation, and the antenna is considered motionless during the emission and reception of the signal. The radiation of waves by moving sources is properly described by Liénard-Wiechert potentials [106, Chapter 8]. In the case of a straightforward uniform motion, the solution can also be obtained using the Lorentz transform, which is done in Chapter 6 for the analysis of the start-stop approximation.

Next, we emphasize that a real-life radar antenna is not a point source, and does not emit the spherically symmetric waves of type (2.4). It rather emits a beam, which has the same functional dependence as (2.4), but is confined to a narrow angular width. To derive the radiation pattern of the antenna, we assume the simplest possible form for the latter, that of a one-dimensional linear segment of length D aligned with the flight track. More precisely, we assume that the center of the antenna is located at $\boldsymbol{x} = (x_1, x_2, x_3) = (x_1, -L, H)$, see Figure 2.1, the antenna itself occupies the interval $[x_1 - D/2, x_1 + D/2]$, and the source density along the antenna is constant. The time-dependent excitation of the antenna is given by the chirp (2.10) so that we have:

$$f(t, \boldsymbol{z}) = P(t)\chi_D(z_1 - x_1)\delta(z_2 - x_2)\delta(z_3 - x_3), \tag{2.16}$$

where similarly to (2.11), χ_D is the indicator function of the interval of length D. We emphasize that unlike (2.3) which is a point source, formula (2.16) defines a line source with constant density, i.e., the density that does not vary in space. While the δ-function in (2.3) has its argument in $\mathbb{R}^3$, both δ-functions in (2.16) have plain real arguments. Accordingly, the meaning of P in formulae (2.16) and (2.3) is also somewhat different. The difference can be seen immediately by comparing the solution of the d'Alembert equation (2.2) driven by the point source (2.3) and given by formula (2.4) with the solution of the same equation (2.2) but driven by the line source (2.16) and given by the Kirchhoff integral:

$$\begin{aligned} u^{(0)}(t, \boldsymbol{z}) &= \frac{1}{4\pi} \iiint\limits_{\mathbb{R}^3} \frac{f(t - |\boldsymbol{z} - \boldsymbol{z}'|/c, \boldsymbol{z}')}{|\boldsymbol{z} - \boldsymbol{z}'|} d\boldsymbol{z}' \\ &= \frac{1}{4\pi} \iiint\limits_{\mathbb{R}^3} \frac{\chi_D(z_1' - x_1)\delta(z_2' - x_2)\delta(z_3' - x_3)}{|\boldsymbol{z} - \boldsymbol{z}'|} P\Big(t - \frac{|\boldsymbol{z} - \boldsymbol{z}'|}{c}\Big) d\boldsymbol{z}' \\ &= \frac{1}{4\pi} \int\limits_{x_1 - D/2}^{x_1 + D/2} \frac{P(t - |\boldsymbol{z} - (z_1', x_2, x_3)|/c)}{|\boldsymbol{z} - (z_1', x_2, x_3)|} dz_1'. \end{aligned} \tag{2.17}$$

Indeed, the final expression for the solution in (2.17) still involves a one-dimensional integration in space while the Kirchhoff integral in (2.4) yields a plain retarded

potential. We, however, will always keep one and the same notation $P = P(t)$ for the chirp regardless of whether it is a point source or a line source, as it is not likely to cause any misunderstanding.

Next, let us denote by γ the angle between the positive direction x_1 and the vector $\boldsymbol{z} - \boldsymbol{x}$, see Figure 2.1. Then, for the point (z_1', x_2, x_3) of the antenna, the cosine law followed by the application of Taylor's formula yields:

$$\begin{aligned} |\boldsymbol{z} - (z_1', x_2, x_3)| &= \sqrt{|\boldsymbol{z} - \boldsymbol{x}|^2 + (z_1' - x_1)^2 - 2(z_1' - x_1)|\boldsymbol{z} - \boldsymbol{x}| \cos\gamma} \\ &\approx |\boldsymbol{z} - \boldsymbol{x}| \left(1 - \frac{(z_1' - x_1)}{|\boldsymbol{z} - \boldsymbol{x}|} \cos\gamma + \frac{(z_1' - x_1)^2}{2|\boldsymbol{z} - \boldsymbol{x}|^2} \sin^2\gamma\right), \end{aligned} \tag{2.18}$$

because $(z_1' - x_1)/|\boldsymbol{z} - \boldsymbol{x}| = \mathcal{O}(D/R) \ll 1$, see Figure 2.1. When substituting approximation (2.18) into the integral (2.17), we take into account that in the definition of the chirp (2.10) the envelope $A(t)$ varies slowly, and that the denominator under the integral on the last line of (2.17) is also a slowly varying function compared to the fast carrier oscillation. Consequently, we can write:

$$\begin{aligned} u^{(0)}(t, \boldsymbol{z}) &\approx \frac{1}{4\pi} \int_{x_1 - D/2}^{x_1 + D/2} \frac{A(t - |\boldsymbol{z} - \boldsymbol{x}|/c)}{|\boldsymbol{z} - \boldsymbol{x}|} e^{-i\omega_0(t - |\boldsymbol{z} - \boldsymbol{x}|/c))} \\ &\qquad \cdot e^{i\omega_0((z_1' - x_1)\cos\gamma - (z_1' - x_1)^2 \sin^2\gamma/2|\boldsymbol{z} - \boldsymbol{x}|)/c} dz_1' \\ &= \frac{1}{4\pi} \frac{P(t - |\boldsymbol{z} - \boldsymbol{x}|/c)}{|\boldsymbol{z} - \boldsymbol{x}|} \int_{-D/2}^{D/2} e^{i\omega_0(\xi\cos\gamma - \xi^2 \sin^2\gamma/2|\boldsymbol{z} - \boldsymbol{x}|)/c} d\xi \\ &= \frac{D}{4\pi} \frac{P(t - |\boldsymbol{z} - \boldsymbol{x}|/c)}{|\boldsymbol{z} - \boldsymbol{x}|} \int_{-1/2}^{1/2} e^{i\omega_0(D\eta\cos\gamma - D^2\eta^2 \sin^2\gamma/2|\boldsymbol{z} - \boldsymbol{x}|)/c} d\eta. \end{aligned}$$

The second term in the exponent under the integral on the last line above can be dropped provided that $\frac{\omega_0}{c}\frac{D^2}{2R} = \frac{\pi D^2}{\lambda_0 R} \ll 1$, where $\lambda_0 = \frac{2\pi c}{\omega_0}$ is the carrier wavelength. This is equivalent to requiring that the target be located in the far-field region of the antenna of size D. (The Fraunhofer distance for this antenna is $\frac{2D^2}{\lambda_0}$.) Then, we have [cf. formula (2.4)]:

$$\begin{aligned} u^{(0)}(t, \boldsymbol{z}) &\approx \frac{D}{4\pi} \frac{P(t - |\boldsymbol{z} - \boldsymbol{x}|/c)}{|\boldsymbol{z} - \boldsymbol{x}|} \int_{-1/2}^{1/2} e^{i\omega_0 D\eta\cos\gamma/c} d\eta \\ &= \frac{D}{4\pi} \frac{P(t - |\boldsymbol{z} - \boldsymbol{x}|/c)}{|\boldsymbol{z} - \boldsymbol{x}|} \frac{\sin(\omega_0 D\cos\gamma/2c)}{\omega_0 D\cos\gamma/2c} \\ &\stackrel{\text{def}}{=} \frac{D}{4\pi} \frac{P(t - |\boldsymbol{z} - \boldsymbol{x}|/c)}{|\boldsymbol{z} - \boldsymbol{x}|} \operatorname{sinc}(\pi D\cos\gamma/\lambda_0). \end{aligned} \tag{2.19}$$

The maximum of the $\operatorname{sinc}(\,\cdot\,)$ on the right-hand side of (2.19) is achieved when the argument is equal to zero, i.e., when $\gamma = \pi/2$. Therefore, the maximum level of radiation emitted by a linear antenna, which is parallel to the orbit, is observed in the direction normal to the orbit. Away from this maximum the radiation level decreases and reaches its minimum where $\operatorname{sinc}(\cdot) = 0$. Hence, it is natural to define the antenna beam as the region between the two zeroes of the $\operatorname{sinc}(\,\cdot\,)$ in (2.19) that are closest to its central maximum. Accordingly, the angular semi-width of the antenna beam (which is centered at the normal direction $\gamma = \pi/2$) is the angle $\Theta/2 = \pi/2 - \gamma$, where γ is such that the sinc in (2.19) attains its first zero. This angle is determined by setting the argument of the $\operatorname{sinc}(\,\cdot\,)$ equal to π: $\pi D \cos(\pi/2 - \Theta/2)/\lambda_0 = \pi$, so that the semi-width of the main lobe of the sinc becomes

$$\sin\frac{\Theta}{2} \approx \frac{\Theta}{2} = \frac{\lambda_0}{D}, \tag{2.20}$$

provided that $\lambda_0/D \ll 1$ so that the approximation $\sin(\Theta/2) \approx \Theta/2$ is valid. Consequently, the full angular width of the antenna beam is $2\lambda_0/D$. The spreading of the beam as it propagates away from the antenna is a manifestation of the well-known phenomenon of diffraction.

Hereafter, we will employ a simplified form of the antenna radiation pattern. Namely, we will assume that the antenna radiates uniformly within the angular width Θ, see formula (2.20), whereas outside of this angle it radiates nothing. In other words, we will replace the $\operatorname{sinc}(\,\cdot\,)$ on the right-hand side of formula (2.19) with the indicator function χ_{Θ}, see (2.11), of the interval $[-\Theta/2, \Theta/2]$:

$$\operatorname{sinc}(\pi D \cos\gamma/\lambda_0) \;\mapsto\; \chi_{\Theta}\Big(\frac{z_1 - x_1}{R}\Big).$$

In the previous formula, we took into account that

$$|\cos\gamma| \approx \frac{|z_1 - x_1|}{R} \leqslant \frac{\lambda_0}{D} \ll 1. \tag{2.21}$$

We also recall that $P(\,\cdot\,)$ in formula (2.19) is the density of a line source. As its length D is much smaller than the distance from the antenna to the target, we can replace $DP(\cdot)$ by the density $P(\cdot)$ of an equivalent point source located at the center of the antenna and radiating within the same angle Θ. Altogether, this yields [cf. formula (2.4)]:

$$u^{(0)}(t, \boldsymbol{z}) \approx \frac{1}{4\pi} \frac{P(t - |\boldsymbol{z} - \boldsymbol{x}|/c)}{|\boldsymbol{z} - \boldsymbol{x}|} \chi_{\Theta}\Big(\frac{z_1 - x_1}{R}\Big). \tag{2.19$'$}$$

In formula (2.19$'$) the subscript "1" denotes the Cartesian coordinate parallel to the flight track, see Figure 2.1.

However, the actual SAR antenna is not one-dimensional. A somewhat more realistic (yet still approximate) model for it would be a planar rectangular frame with one of its sides parallel to the flight track (orbit) and the normal to the plane

pointing in the direction of incidence, i.e., making the angle θ with the vertical axis, see Figure 2.1. This model allows one to introduce both the horizontal and vertical radiation pattern of the antenna. The horizontal pattern is the one discussed in this section, see (2.19), (2.20), and (2.19′); it determines the size of the beam footprint along the flight track, i.e., in the azimuthal direction. The analysis for the vertical radiation pattern is also the same as presented here (see, e.g., [86]), and the result naturally coincides with (2.20) — the angular width of the beam will be given by the ratio of the wavelength to the antenna size in the direction normal to the orbit. Clearly, the angular width of the beam in the vertical direction, along with the look angle θ, determines the size of the beam footprint across the flight track, i.e., in the range direction, and as such, the width of the swath in the stripmap imaging scenario, see Figure 2.1.

A finite size of the beam footprint on the ground implies that the integration area in formula (2.9) needs to be restricted accordingly. In other words, the integration with respect to $\boldsymbol{z}$ that yields the scattered field at $\boldsymbol{x}'$ shall be performed only over the region illuminated by the antenna. As such, the integration limits in (2.9) shall be introduced in both the azimuthal and range direction. Subsequently, they will be inherited in (2.14″). For clarity, however, we will keep the following simplified expression for $u^{(1)}$ obtained by substituting (2.19′) into (2.9) and carrying out the same derivation as in Section 2.1:

$$u^{(1)}(t,\boldsymbol{x}) \approx \int v(\boldsymbol{z}) P\left(t-2|\boldsymbol{x}-\boldsymbol{z}|/c\right) \chi_{\Theta}\Big(\frac{z_1-x_1}{R}\Big) d\boldsymbol{z}. \tag{2.22}$$

Formula (2.22) explicitly specifies only the integration limits in azimuth by means of the indicator function $\chi_{\Theta}(\,\cdot\,)$. The reason is that the size of the beam footprint in the azimuthal direction plays an additional very important role as it determines the maximum size of the synthetic aperture, see Section 2.3.2.

2.3 Inversion of the raw data

2.3.1 Matched filter

To solve the inverse scattering problem for SAR would mean to obtain $v(\boldsymbol{z})$ from the known $u^{(1)}(t,\boldsymbol{x})$. In other words, one needs to invert the integral operator that acts on $v(\boldsymbol{z})$ on the right-hand side of (2.22). The approximate inversion, which is also called the SAR signal processing, is done in two stages. First, the received antenna signal $u^{(1)}(t,\boldsymbol{x})$ given by (2.22) is multiplied by the function

$$\overline{P(t-2|\boldsymbol{y}-\boldsymbol{x}|/c)} = \chi_{\tau}(t-2|\boldsymbol{y}-\boldsymbol{x}|/c) e^{i\alpha(t-2|\boldsymbol{y}-\boldsymbol{x}|/c)^2} e^{i\omega_0(t-2|\boldsymbol{y}-\boldsymbol{x}|/c)}, \tag{2.23}$$

where $\boldsymbol{y}$ is a parameter, and the result is integrated with respect to t:

$$\begin{aligned} I_{\boldsymbol{x}}(\boldsymbol{y}) &= \int_{\chi} \overline{P(t-2R_y/c)} u^{(1)}(t,\boldsymbol{x})\, dt \\ &= \int d\boldsymbol{z}\, v(\boldsymbol{z}) \chi_{\Theta}\Big(\frac{z_1-x_1}{R}\Big) \underbrace{\int_{\chi} dt\, \overline{P(t-2R_y/c)} P(t-2R_z/c)}_{W_{\boldsymbol{x}}(\boldsymbol{y},\boldsymbol{z})}, \end{aligned} \tag{2.24}$$

where

$$R_y \overset{\text{def}}{=} |\boldsymbol{y}-\boldsymbol{x}| \quad \text{and} \quad R_z \overset{\text{def}}{=} |\boldsymbol{z}-\boldsymbol{x}|.$$

In formulae (2.23) and (2.24), the overbar denotes a complex conjugate. In the radar literature, the operation of (2.24) is commonly referred to as application of the matched filter, see, e.g., [79, Section 3.1.1] or [110, Section 1.2]. The filter (2.23) is called matched because it is also a chirp with the same duration τ, rate α, and carrier frequency ω_0 as the original chirp (2.10), (2.11), and in the case where $R_y = R_z$ the phase of the expression on the right-hand side of (2.23) is exactly the opposite to the phase of the received signal $P(t-2R_z/c)$. The rationale behind choosing the matched filter in the form (2.23) is presented in Appendix 2.A. Note also that while in our analysis the matched filter is considered only as a part of the inversion algorithm, it can also be shown that it provides the best signal-to-noise ratio in the sense of L_2 in the case where the inversion is done in the presence of noise, see [9, Section 4.1] and also [110].

The interior integral $W_{\boldsymbol{x}}(\boldsymbol{y},\boldsymbol{z})$ on the right-hand side of (2.24) is known as the point spread function (PSF), and the notation $\int_{\chi} dt$ means that the integration limits are determined by the indicator function(s) χ_{τ} under the integral, see (2.10) and (2.11). Given the notation $W_{\boldsymbol{x}}(\boldsymbol{y},\boldsymbol{z})$ for the PSF, the image $I_{\boldsymbol{x}}$ for a single pulse emitted from the point $\boldsymbol{x}$ becomes:

$$I_{\boldsymbol{x}}(\boldsymbol{y}) = \int W_{\boldsymbol{x}}(\boldsymbol{y},\boldsymbol{z}) v(\boldsymbol{z}) \chi_{\Theta}\Big(\frac{z_1-x_1}{R}\Big)\, d\boldsymbol{z}. \tag{2.25}$$

2.3.2 Synthetic aperture

The next stage of inversion is to consider a sequence of radar pulses emitted at times t_n from the equally spaced positions $\boldsymbol{x}^n = (x_1^n, -L, H)$, as the antenna moves along the linear flight track (orbit), see Figure 2.1. Recall that under the start-stop approximation, the n-th pulse is emitted, and the scattered response is received, when the antenna is at standstill at the position $\boldsymbol{x}^n$, after which it moves to the next emitting/receiving position. Let Δx_1 denote the distance along the flight track between the successive emitting/receiving positions of the antenna. Then, we can write:

$$\Delta x_1 = \mathfrak{v}\tau_{\mathrm{p}}, \tag{2.26}$$

where $\mathfrak{v}$ is the platform velocity and $\tau_p = t_n - t_{n-1}$ is the time interval between two consecutive pulses. The reciprocal of τ_p is known as the pulse repetition frequency (PRF):

$$f_p \stackrel{\text{def}}{=} \frac{1}{\tau_p}. \tag{2.27}$$

We also assume that the pulses are emitted toward the ground in the direction normal to the platform trajectory. This corresponds to the broadside stripmap SAR imaging, see Figure 2.1.

The range of values of n in the foregoing sequence of pulses is determined by the geometry of the antenna beam discussed in Section 2.2. For a given reference location $\boldsymbol{y} = (y_1, y_2, 0)$ on the ground (i.e., for a given image point), consider those and only those $\boldsymbol{x}^n = (x_1^n, -L, H)$, for which this location remains within the footprint of the antenna beam, see Figure 2.1. In other words, according to (2.20), we consider those and only those $\boldsymbol{x}^n$ for which

$$y_1 - \frac{\lambda_0}{D}R \leqslant x_1^n \leqslant y_1 + \frac{\lambda_0}{D}R, \tag{2.28a}$$

or, equivalently,

$$\frac{y_1}{\Delta x_1} - \frac{N}{2} \leqslant n \leqslant \frac{y_1}{\Delta x_1} + \frac{N}{2}, \quad \text{where} \quad N = \left[\frac{2\lambda_0 R}{\Delta x_1 D}\right]. \tag{2.28b}$$

In formula (2.28b), $[\cdot]$ is the notation for the integer part and Δx_1 is given by (2.26). By defining the length of the synthetic aperture as

$$L_{SA} \approx \Theta R = 2\frac{\lambda_0}{D}R, \tag{2.29}$$

we recast (2.28a) as

$$y_1 - \frac{L_{SA}}{2} \leqslant x_1^n \leqslant y_1 + \frac{L_{SA}}{2}, \tag{2.30a}$$

and redefine N of (2.28b) as

$$N = \left[\frac{L_{SA}}{\Delta x_1}\right] = \left[\frac{L_{SA}}{\mathfrak{v}} f_p\right], \tag{2.30b}$$

where the PRF f_p is given by (2.27). In practice, the length of the synthetic aperture may be chosen smaller than (2.29), i.e., $L_{SA} < 2\lambda_0 R/D$, especially when the carrier frequency ω_0 is not very high and hence the wavelength $\lambda_0 = 2\pi c/\omega_0$ is relatively large. Then, the number of terms N given by (2.30b) in the sequence (2.30a) changes accordingly.

The full SAR image $I(\boldsymbol{y})$ is a coherent sum of the contributions $I_{\boldsymbol{x}^n}(\boldsymbol{y})$ along the synthetic aperture, where each $I_{\boldsymbol{x}^n}(\boldsymbol{y})$ is given by (2.25) for $\boldsymbol{x} = \boldsymbol{x}^n$. As the set of x_1^n within the synthetic aperture is defined by (2.30a), it is convenient to introduce the summation limits with the help of the indicator function:

$$\chi_{L_{\mathrm{SA}}}(y_1 - x_1^n) = \begin{cases} 1, & \text{if } x_1^n \text{ satisfies (2.30a)}, \\ 0, & \text{otherwise.} \end{cases}$$

Then,

$$\begin{aligned} I(\boldsymbol{y}) &= \sum_n \chi_{L_{\mathrm{SA}}}(y_1 - x_1^n) I_{\boldsymbol{x}^n}(\boldsymbol{y}) \\ &= \sum_n \chi_{L_{\mathrm{SA}}}(y_1 - x_1^n) \int W_{\boldsymbol{x}^n}(\boldsymbol{y}, \boldsymbol{z}) v(\boldsymbol{z}) \chi_\Theta\Big(\frac{z_1 - x_1^n}{R}\Big) d\boldsymbol{z} \\ &= \int \Big[\sum_n \chi_{L_{\mathrm{SA}}}(y_1 - x_1^n) \chi_{L_{\mathrm{SA}}}(z_1 - x_1^n) W_{\boldsymbol{x}^n}(\boldsymbol{y}, \boldsymbol{z}) \Big] v(\boldsymbol{z})\, d\boldsymbol{z} \\ &= \int W(\boldsymbol{y}, \boldsymbol{z}) v(\boldsymbol{z})\, d\boldsymbol{z} = W * v, \end{aligned} \tag{2.31}$$

where we took into account that according to (2.20) and (2.29), $\chi_\Theta\big(\frac{z_1 - x_1^n}{R}\big) \equiv \chi_{L_{\mathrm{SA}}}(z_1 - x_1^n)$. While each $\boldsymbol{x}^n$ in the sum (2.31) is the location of the antenna at the physical moment of time t_n, the summation index n is often referred to as the "slow time" in the SAR literature,[4] see, e.g., [9, Chapter 9].

2.3.3 Imaging kernel

The function $W(\boldsymbol{y}, \boldsymbol{z})$ on the last line of (2.31) is obtained by summing up all the PSFs $W_{\boldsymbol{x}^n}(\boldsymbol{y}, \boldsymbol{z})$:

$$\begin{aligned} W(\boldsymbol{y}, \boldsymbol{z}) &= \sum_n \chi_{L_{\mathrm{SA}}}(y_1 - x_1^n) \chi_{L_{\mathrm{SA}}}(z_1 - x_1^n) W_{\boldsymbol{x}^n}(\boldsymbol{y}, \boldsymbol{z}) \\ &= \sum_n \chi_{L_{\mathrm{SA}}}(y_1 - x_1^n) \chi_{L_{\mathrm{SA}}}(z_1 - x_1^n) \end{aligned}$$

[4] As opposed to the physical, or "fast," time t in formulae (2.24) and (2.32).

$$\int_\chi dt\, \overline{P(t-t_n-2R_y^n/c)}P(t-t_n-2R_z^n/c) \tag{2.32}$$
$$= \sum_n \chi_{L_{\mathrm{SA}}}(y_1-x_1^n)\chi_{L_{\mathrm{SA}}}(z_1-x_1^n)e^{2i\omega_0(R_z^n/c-R_y^n/c)}$$
$$\int_\chi dt\, \overline{A(t-t_n-2R_y^n/c)}A(t-t_n-2R_z^n/c),$$

where

$$R_y^n = |\boldsymbol{y}-\boldsymbol{x}^n| \quad \text{and} \quad R_z^n = |\boldsymbol{z}-\boldsymbol{x}^n|. \tag{2.33}$$

For any choice of y_1 and z_1, the summation range in (2.32) is clearly finite.

The imaging kernel $W(\boldsymbol{y},\boldsymbol{z})$ of (2.32) is often called the generalized ambiguity function (GAF). Due to the integral representation on the last line of (2.31), $W(\boldsymbol{y},\boldsymbol{z}_0)$ for a given $\boldsymbol{z}_0$ can formally be thought of as the image $I(\boldsymbol{y})$ of a point source $\nu(\boldsymbol{z}) = \delta(\boldsymbol{z}-\boldsymbol{z}_0)$. In the end of Section 2.6, we show that W can be expressed as $W(\boldsymbol{y},\boldsymbol{z}) = W(\boldsymbol{y}-\boldsymbol{z})$, which justifies the convolution notation $W*\nu$ for the last integral in (2.31). Note also that formula (2.1) for the image discussed in the beginning of this chapter coincides with (2.31).

If the foregoing SAR data inversion algorithm were exact, then the imaging kernel W would coincide with the δ-function, $W(\boldsymbol{y}-\boldsymbol{z}) = \delta(\boldsymbol{y}-\boldsymbol{z})$, which, in turn, would imply that $I = W*\nu = \delta*\nu = \nu$. In reality, however, the inversion is only approximate rather than exact, the kernel W is not a δ-function, and the image does not, generally speaking, coincide with the ground reflectivity.

To quantify the discrepancies between the ground reflectivity function $\nu(\boldsymbol{z})$ of (2.15′) and the image $I(\boldsymbol{y})$ of (2.31), one should therefore study the properties of the imaging kernel, i.e., of the GAF $W(\boldsymbol{y},\boldsymbol{z})$ given by (2.32). The GAF is computed in Section 2.4 and analyzed further in Sections 2.5 and 2.6.

2.4 The generalized ambiguity function

2.4.1 Factorized representation of the GAF

We first notice that in each individual term of the sum (2.32), $t-t_n$ can be replaced with t by merely changing the integration variable. The remaining dependence of $\overline{A(t-2R_y^n/c)}$ and $A(t-2R_z^n/c)$ on n is through $\boldsymbol{x}^n$, see (2.33); it is weak because A in (2.10) is a slowly varying envelope itself. Hence, we can take $\overline{A(\cdot)}$ and $A(\cdot)$ out of the summation over n, so that the GAF $W(\boldsymbol{y},\boldsymbol{z})$ of (2.32) can approximately be represented as a product of two factors:

$$W(\boldsymbol{y},\boldsymbol{z}) \approx W_\Sigma(\boldsymbol{y},\boldsymbol{z})\cdot W_{\mathrm{R}}(\boldsymbol{y},\boldsymbol{z}), \tag{2.34}$$

where

$$W_\Sigma(\boldsymbol{y},\boldsymbol{z}) = \sum_n \chi_{L_{\mathrm{SA}}}(y_1 - x_1^n)\chi_{L_{\mathrm{SA}}}(z_1 - x_1^n)e^{2ik_0(R_z^n - R_y^n)} \tag{2.35}$$

and

$$W_{\mathrm{R}}(\boldsymbol{y},\boldsymbol{z}) = \int_\chi \overline{A(t - 2R_y^{\mathrm{c}}/c)}A(t - 2R_z^{\mathrm{c}}/c)\,dt. \tag{2.36}$$

In (2.35), $k_0 = \omega_0/c$ is the carrier wavenumber. In (2.36), we have [cf. formula (2.33)]:

$$R_y^{\mathrm{c}} = |\boldsymbol{y} - \boldsymbol{x}^{n_{\mathrm{c}}}| \quad \text{and} \quad R_z^{\mathrm{c}} = |\boldsymbol{z} - \boldsymbol{x}^{n_{\mathrm{c}}}|, \tag{2.37}$$

where $\boldsymbol{x}^{n_{\mathrm{c}}}$ is the position of the antenna that corresponds to the center of the summation interval defined by the product of the two indicator functions under the sum in (2.35). The actual value of n_{c} is introduced later, see formula (2.43).

We now proceed with the evaluation of the individual factors (2.35) and (2.36). In Section 2.5, we also estimate the factorization error, i.e., the error of replacing the GAF (2.32) with its approximate representation (2.34). This error proves to be small, on the order of the relative bandwidth, i.e., about B/ω_0.

2.4.2 Azimuthal sum and pulse repetition frequency

To evaluate the azimuthal factor (2.35), we first need to identify and verify an important constraint for the pulse repetition frequency (2.27) or, equivalently, the time interval τ_{p} between two consecutive pulses, see (2.26). Let us linearize the travel distances R_y^n and R_z^n of (2.33), see Figure 2.1. With no loss of generality we assume that $z_2 = 0$ and also denote $y_2 - z_2 = y_2 = l$ for convenience. Then, we can write:

$$\begin{aligned} R_z^n &= \left(H^2 + L^2 + (x_1^n - z_1)^2\right)^{1/2} = \left(R^2 + (x_1^n - z_1)^2\right)^{1/2} \\ &= R\left(1 + \frac{(x_1^n - z_1)^2}{R^2}\right)^{1/2} \approx R + \frac{1}{2}\frac{(x_1^n - z_1)^2}{R} \end{aligned} \tag{2.38}$$

and

$$\begin{aligned} R_y^n &= \left(H^2 + (L+l)^2 + (x_1^n - y_1)^2\right)^{1/2} = \left(R^2 + 2Ll + l^2 + (x_1^n - y_1)^2\right)^{1/2} \\ &= R\left(1 + \frac{2Ll + l^2 + (x_1^n - y_1)^2}{R^2}\right)^{1/2} \end{aligned}$$

$$\approx R\left(1+\frac{1}{2}\frac{2Ll+l^2+(x_1^n-y_1)^2}{R^2}-\frac{1}{8}\frac{4L^2l^2}{R^4}\right)$$
$$=R+\frac{1}{2}\frac{2Ll+l^2\cos^2\theta+(x_1^n-y_1)^2}{R}, \tag{2.39}$$

where we took into account that $1-L^2/R^2=\cos^2\theta$, see Figure 2.1. Subtracting equation (2.39) from equation (2.38), we have:

$$\begin{aligned} R_z^n-R_y^n &\approx \frac{(x_1^n-z_1)^2-2Ll-l^2\cos^2\theta-(x_1^n-y_1)^2}{2R} \\ &= \frac{z_1^2-y_1^2-2Ll-l^2\cos^2\theta+2(y_1-z_1)x_1^n}{2R} \\ &= -\frac{Ll}{R}+\frac{z_1^2-y_1^2-l^2\cos^2\theta}{2R}+\frac{(y_1-z_1)x_1^n}{R}. \end{aligned} \tag{2.40}$$

Recalling that $x_1^n=n\Delta x_1=nL_{\rm SA}/N$, for the sum (2.35) we have:

$$W_\Sigma(\boldsymbol{y},\boldsymbol{z})=\chi_{2L_{\rm SA}}(y_1-z_1)\sum_{n=N_1(\boldsymbol{y},\boldsymbol{z})}^{N_2(\boldsymbol{y},\boldsymbol{z})}e^{2ik_0(R_z^n-R_y^n)}, \tag{2.41}$$

where the summation limits are defined according to (2.28b) and (2.30):

$$\begin{aligned} N_1(\boldsymbol{y},\boldsymbol{z}) &= \left[\frac{\max(y_1,z_1)}{\Delta x_1}-\frac{L_{\rm SA}}{2\Delta x_1}\right], \\ N_2(\boldsymbol{y},\boldsymbol{z}) &= \left[\frac{\min(y_1,z_1)}{\Delta x_1}+\frac{L_{\rm SA}}{2\Delta x_1}\right], \end{aligned} \tag{2.42}$$

and the indicator function $\chi_{2L_{\rm SA}}(y_1-z_1)$ in front of the sum in (2.41) accounts for the fact that if $|y_1-z_1|>L_{\rm SA}$, then the intervals defined by $\chi_{L_{\rm SA}}(y_1-x_1^n)$ and $\chi_{L_{\rm SA}}(z_1-x_1^n)$ on the right-hand side of (2.35) do not overlap, the summation range is empty, and the sum is equal to zero. To symmetrize the summation interval in (2.41) in the case of a nonempty overlap, we introduce

$$n_{\rm c}=\left[\frac{y_1+z_1}{2\Delta x_1}\right],\quad \tilde{n}=n-n_{\rm c},\quad \text{and}\quad \tilde{N}=N-\left[\frac{|y_1-z_1|}{\Delta x_1}\right], \tag{2.43}$$

where $n_{\rm c}$ is the center of the interval and $\tilde{N}$ is the number of terms in the sum that represents $W_\Sigma(\boldsymbol{y},\boldsymbol{z})$. In doing so, we note that the sum that yields the image $I(\boldsymbol{y})$ for a given $\boldsymbol{y}$, see the first line of (2.31), is not identical to the sum that yields the imaging kernel $W(\boldsymbol{y},\boldsymbol{z})$ of (2.32) and, accordingly, the factor $W_\Sigma(\boldsymbol{y},\boldsymbol{z})$ of (2.35). For the former, the center of the synthetic aperture is at y_1 so that the center of the summation interval is at $\left[\frac{y_1}{\Delta x_1}\right]$, and the number of terms in the sum is N, see

formulae (2.28b) and (2.30). For the latter, the center of the summation interval is at $n = n_c$ given by (2.43), which corresponds to the midpoint between y_1 and z_1, and the number of terms is $\tilde{N}$. The quantity n_c is also used in the definition of R_y^c and R_z^c, see (2.37), that appear in the factor $W_R(\boldsymbol{y}, \boldsymbol{z})$ of (2.36). We will see shortly that $N \gg 1$, see (2.50); for this reason, we will often ignore the fractional part in expressions such as (2.43) and (2.28b).

Substituting (2.40) and (2.43) into (2.41) and assuming $\tilde{N}$ to be even, we obtain:

$$\begin{aligned} W_\Sigma(\boldsymbol{y}, \boldsymbol{z}) &= e^{-2ik_0 \frac{Ll}{R}} e^{ik_0 \frac{z_1^2 - y_1^2 - l^2 \cos^2\theta}{R}} \chi_{2L_{SA}}(y_1 - z_1) \\ &\quad \cdot \sum_{\tilde{n}=-\tilde{N}/2}^{\tilde{N}/2} e^{2ik_0(y_1 - z_1)L_{SA}(\tilde{n}+n_c)/(RN)} \\ &= e^{-2ik_0 \frac{Ll}{R}} e^{-ik_0 \frac{l^2 \cos^2\theta}{R}} \chi_{2L_{SA}}(y_1 - z_1) \\ &\quad \cdot \sum_{\tilde{n}=-\tilde{N}/2}^{\tilde{N}/2} e^{2ik_0(y_1 - z_1)L_{SA}\tilde{n}/(RN)}. \end{aligned} \tag{2.44}$$

On the last line of (2.44), we have the sum of a geometric sequence:

$$\sum_{\tilde{n}=-\tilde{N}/2}^{\tilde{N}/2} e^{i\tilde{n}\varphi} = \frac{\sin(\varphi(\tilde{N}+1)/2)}{\sin(\varphi/2)}, \tag{2.45}$$

where

$$\varphi = 2k_0(y_1 - z_1)\frac{L_{SA}}{RN}. \tag{2.46}$$

The function on the right-hand side of (2.45) is a periodic function of its argument $\varphi/2$ with the period 2π determined by the denominator. In accordance with (2.46), it is also a periodic function of the argument $(y_1 - z_1)$ with the period X defined as

$$X = \frac{2\pi}{k_0}\frac{RN}{L_{SA}} = \frac{\lambda_0 RN}{L_{SA}}, \tag{2.47}$$

where λ_0 is the carrier wavelength. The function (2.45) has a distinct peak between the two zeroes of the numerator closest to the center: $\varphi(\tilde{N}+1)/2 = \pm\pi$, with the maximum reached at $\varphi = 0 \Leftrightarrow y_1 = z_1$, i.e., where the denominator on the right-hand side of (2.45) turns into zero. This peak is often referred to as the main lobe. Due to the periodicity, the function (2.45) also has infinitely many identical peaks separated by the distance X of (2.47). Those are called the grating lobes, see, e.g., [40, Section 1.4.2].

The periodicity of (2.45) imposes the following constraint on the pulse repetition frequency. Namely, we would like the azimuthal factor of the GAF (2.44)

$$W_\Sigma(\boldsymbol{y},\boldsymbol{z}) = e^{-2ik_0\frac{Ll}{R}}e^{-ik_0\frac{l^2\cos^2\theta}{R}}\chi_{2L_{\mathrm{SA}}}(y_1-z_1)\frac{\sin(\varphi(\tilde{N}+1)/2)}{\sin(\varphi/2)} \tag{2.48}$$

to have only one main lobe and no grating lobes. This is possible when the period X of (2.47) is greater than the synthetic aperture L_{SA}:

$$X > L_{\mathrm{SA}}, \tag{2.49}$$

because in this case the grating lobes of (2.45) are cut off by the indicator function $\chi_{2L_{\mathrm{SA}}}(y_1 - z_1)$ on the right-hand side of (2.48).[5] Inequality (2.49) along with the definition (2.47) yields:

$$N > \frac{L_{\mathrm{SA}}^2}{\lambda_0}\frac{1}{R} \gg 1. \tag{2.50}$$

The first fraction on the right-hand side of (2.50) is half the Fraunhofer distance of the synthetic array. It is much larger than the distance R between the antenna and the target, because the target is in the near field of the array. Equivalently, relation (2.49) with the help of (2.26), (2.27), and (2.30b) can be recast as:

$$\tau_{\mathrm{p}} < \frac{L_{\mathrm{SA}}}{\mathfrak{v}}\cdot\frac{\lambda_0 R}{L_{\mathrm{SA}}^2} \tag{2.51a}$$

or

$$f_{\mathrm{p}} > \frac{\mathfrak{v}}{L_{\mathrm{SA}}}\cdot\frac{L_{\mathrm{SA}}^2}{\lambda_0 R}. \tag{2.51b}$$

Inequality (2.51a) is an upper bound for the time interval between the consecutive pulses, while inequality (2.51b) is its reciprocal lower bound for the PRF. These bounds guarantee that the period X satisfies (2.49), which, in turn, removes the grating lobes from the azimuthal factor of the GAF (2.48). For the typical values of the parameters presented in Table 1.1, inequality (2.51a) holds with a safe margin since $\tau_{\mathrm{p}} = 5\cdot 10^{-4}s$ whereas the right-hand side of (2.51a) is approximately equal to $2.56\cdot 10^{-3}s$.

[5] Grating lobes are responsible for the appearance of "ghost" images of bright targets shifted in azimuth with respect to their true location $y_1 = z_1$. Since the indicator function is only an approximation to the true antenna radiation pattern (see formulae (2.19) and (2.19′)), then in reality, the choice of the period X satisfying (2.49) will reduce the amplitude of grating lobes but not completely eliminate them.

For the common imaging configurations (see Table 1.1) we have $k_0\frac{L_{\mathrm{SA}}}{N} = \frac{2\pi\mathfrak{v}\tau_{\mathrm{p}}}{\lambda_0} > 1$, which means that the distance between the successive emitting/receiving locations of the antenna is greater than the carrier wavelength. Therefore, for the entire range of $(y_1 - z_1)$ for which the right-hand side of (2.48) may be nonzero, i.e., for y_1 and z_1 within the beam footprint, $|y_1 - z_1| < L_{\mathrm{SA}}$, we have $|\varphi| \lesssim 1$ according to (2.46) because $L_{\mathrm{SA}} \ll R$. In practice, we are predominantly interested in evaluating $W_\Sigma(\boldsymbol{y}, \boldsymbol{z})$ for the locations $\boldsymbol{y}$ and $\boldsymbol{z}$ that are sufficiently close to one another, i.e., $|y_1 - z_1| \ll L_{\mathrm{SA}}$. Then, it is easy to see that $|\varphi| \ll 1$ and we can therefore replace the sine function by its argument in the denominator on the right-hand side of (2.45), $\sin(\varphi/2) \approx \varphi/2$. Moreover, for $|y_1 - z_1| \ll L_{\mathrm{SA}}$ the relative difference between N and $\tilde{N}$ is small, see (2.43), and since $N \gg 1$ according to (2.50), we have $\tilde{N} \gg 1$. Altogether, this yields:

$$\sum_{\tilde{n}=-\tilde{N}/2}^{\tilde{N}/2} e^{i\tilde{n}\varphi} \approx \frac{\sin(\varphi\tilde{N}/2)}{\varphi/2} = \tilde{N}\frac{\sin(\varphi\tilde{N}/2)}{\tilde{N}\varphi/2} = \tilde{N}\,\mathrm{sinc}\,\frac{\tilde{N}\varphi}{2}. \tag{2.52}$$

Unlike (2.45), the sinc function on the right-hand side of (2.52) is not periodic. It has one main lobe between $\tilde{N}\varphi/2 = \pm\pi$ with the maximum at $\varphi = 0$ and a series of sidelobes that decay as $|\varphi|$ increases. The approximation of (2.45) by (2.52) is accurate for $|y_1 - z_1| \ll L_{\mathrm{SA}}$. It is acceptable for the entire range of admissible y_1 and z_1 though, $|y_1 - z_1| < L_{\mathrm{SA}}$, because we still have $|\varphi| \lesssim 1$.

In subsequent chapters of the book, we will be computing azimuthal sums similar to (2.35) on multiple occasions. In doing so, we will automatically disregard the grating lobes based on the argument presented in this section.

2.4.3 The azimuthal factor

To complete the derivation of the azimuthal factor $W_\Sigma(\boldsymbol{y}, \boldsymbol{z})$, we notice that the second exponent on the right-hand side of (2.48) is much smaller than the first one, and hence we ignore it. Then, using formulae (2.43), (2.46), (2.48), and (2.52), we can write:

$$\begin{aligned} W_\Sigma(\boldsymbol{y}, \boldsymbol{z}) &\approx e^{-2ik_0\frac{U}{R}}\tilde{N}\,\mathrm{sinc}\left(k_0(y_1 - z_1)\frac{L_{\mathrm{SA}}}{R}\frac{\tilde{N}}{N}\right) \\ &= e^{-2ik_0\frac{U}{R}}\tilde{N}\,\mathrm{sinc}\left(\frac{k_0 L_{\mathrm{SA}}}{R}(y_1 - z_1)\Big(1 - \frac{|y_1 - z_1|}{N\Delta x_1}\Big)\right). \end{aligned} \tag{2.53}$$

The sinc function in (2.53) reaches its maximum value when $y_1 = z_1$, i.e., when the argument of the $\mathrm{sinc}(\cdot)$ is equal to zero. We also note that the argument of the $\mathrm{sinc}(\cdot)$ in (2.53) becomes zero not only for $y_1 = z_1$ but also for $|y_1 - z_1| = N\Delta x_1$. However, the overall function $\tilde{N}\,\mathrm{sinc}(\cdot)$ does not have a peak there because according to (2.52), at this second zero of the argument only the numerator of $\frac{\sin(\varphi\tilde{N}/2)}{\varphi/2} \equiv \tilde{N}\frac{\sin(\varphi\tilde{N}/2)}{\tilde{N}\varphi/2}$ is zero while the denominator is not. Besides, we are mostly interested in the case $|y_1 - z_1| \ll L_{\mathrm{SA}} = N\Delta x_1$.

Furthermore, the $\operatorname{sinc}(\cdot)$ in (2.53) reaches its first zero (closest to the maximum) when the argument is equal to π. To find the location of the first zero, we need to solve the equation

$$\frac{k_0 L_{\mathrm{SA}}}{R}(y_1 - z_1)\Big(1 - \frac{y_1 - z_1}{L_{\mathrm{SA}}}\Big) = \pi, \tag{2.54}$$

where we have substituted $N\Delta x_1 = L_{\mathrm{SA}}$ and also replaced $|y_1 - z_1|$ with $y_1 - z_1$ with no loss of generality, because the other case is analyzed similarly. Equation (2.54) is quadratic with respect to $y_1 - z_1$ and has the roots:

$$\begin{aligned} y_1 - z_1 &= \frac{R}{2k_0}\left(\frac{k_0 L_{\mathrm{SA}}}{R} \mp \frac{k_0 L_{\mathrm{SA}}}{R}\sqrt{1 - \frac{4\pi R}{k_0 L_{\mathrm{SA}}^2}}\right) \\ &\approx \frac{R}{2k_0}\left(\frac{k_0 L_{\mathrm{SA}}}{R} \mp \frac{k_0 L_{\mathrm{SA}}}{R}\Big(1 - \frac{2\pi R}{k_0 L_{\mathrm{SA}}^2}\Big)\right). \end{aligned} \tag{2.55}$$

Note that we have approximated the square root on the first line of (2.55) with its first order Taylor expansion on the second line of (2.55) because

$$\frac{R}{k_0 L_{\mathrm{SA}}^2} = \frac{R}{\pi}\left(\frac{2L_{\mathrm{SA}}^2}{\lambda_0}\right)^{-1} \ll 1. \tag{2.56}$$

Indeed, the quantity $2L_{\mathrm{SA}}^2/\lambda_0$ is the Fraunhofer distance of the synthetic array, which is much greater than the distance R from the antenna to the target, see Table 1.2.

The first one of the two roots (2.55) is

$$y_1 - z_1 = \frac{\pi R}{k_0 L_{\mathrm{SA}}} = \frac{\pi R c}{\omega_0 L_{\mathrm{SA}}} \stackrel{\mathrm{def}}{=} \Delta_{\mathrm{A}}. \tag{2.57}$$

For the root (2.57), we clearly have $\Delta_{\mathrm{A}} \ll L_{\mathrm{SA}}$ due to the same argument (2.56). The second root (2.55) is given by

$$y_1 - z_1 = \frac{R}{2k_0}\left(\frac{k_0 L_{\mathrm{SA}}}{R} - \frac{1}{L_{\mathrm{SA}}}\right) = L_{\mathrm{SA}} - \Delta_{\mathrm{A}}.$$

It is of no interest for subsequent consideration though, because it does not satisfy the assumption $|y_1 - z_1| \ll L_{\mathrm{SA}}$.

The main lobe of the $\operatorname{sinc}(\cdot)$ in formula (2.53) is located on the interval between its two closest zeros on both sides of the central maximum: $[-\Delta_{\mathrm{A}}, \Delta_{\mathrm{A}}]$. Within the main lobe, we can obviously replace $\tilde{N}$ with N and obtain the following expression for W_Σ:

$$\begin{aligned} W_\Sigma(\boldsymbol{y}, \boldsymbol{z}) &\approx e^{-2ik_0\frac{U}{R}} N \operatorname{sinc}(k_0(y_1 - z_1)L_{\mathrm{SA}}/R) \\ &= e^{-2ik_0\frac{U}{R}} N \operatorname{sinc}\left(\pi\frac{y_1 - z_1}{\Delta_{\mathrm{A}}}\right) \stackrel{\mathrm{def}}{=} e^{-2ik_0\frac{U}{R}} W_{\mathrm{A}}(\boldsymbol{y}, \boldsymbol{z}). \end{aligned} \tag{2.58}$$

Note that the transition from (2.53) to (2.58) involves replacing $\tilde{N}$ by N not only in the argument of the sinc(·) but also in front of the sinc(·). This, however, implies only a very small, and thus inconsequential, change in the amplitude.

2.4.4 The range factor

The range factor (2.36) of the GAF is given by

$$\begin{aligned} W_{\mathrm{R}}(\boldsymbol{y},\boldsymbol{z}) &= \int_{\chi} \overline{A(t-2R_{\boldsymbol{y}}^{\mathrm{c}}/c)}A(t-2R_{\boldsymbol{z}}^{\mathrm{c}}/c)\,dt \\ &= \int_{\chi} \chi_{\tau}(t-2R_{\boldsymbol{y}}^{\mathrm{c}}/c)e^{i\alpha(t-2R_{\boldsymbol{y}}^{\mathrm{c}}/c)^2}\chi_{\tau}(t-2R_{\boldsymbol{z}}^{\mathrm{c}}/c)e^{-i\alpha(t-2R_{\boldsymbol{z}}^{\mathrm{c}}/c)^2}dt \\ &= \int_{\max\{2R_{\boldsymbol{y}}^{\mathrm{c}}/c,2R_{\boldsymbol{z}}^{\mathrm{c}}/c\}-\tau/2}^{\min\{2R_{\boldsymbol{y}}^{\mathrm{c}}/c,2R_{\boldsymbol{z}}^{\mathrm{c}}/c\}+\tau/2} e^{i\alpha(t-2R_{\boldsymbol{y}}^{\mathrm{c}}/c)^2}e^{-i\alpha(t-2R_{\boldsymbol{z}}^{\mathrm{c}}/c)^2}dt. \end{aligned}$$

In the last integral, we change the integration variable: $\tilde{t} = t - (R_{\boldsymbol{y}}^{\mathrm{c}} + R_{\boldsymbol{z}}^{\mathrm{c}})/c$, and also denote $T^{\mathrm{c}} = (R_{\boldsymbol{y}}^{\mathrm{c}} - R_{\boldsymbol{z}}^{\mathrm{c}})/c$ so that

$$t - \frac{2R_{\boldsymbol{y}}^{\mathrm{c}}}{c} = \tilde{t} - T^{\mathrm{c}} \quad \text{and} \quad t - \frac{2R_{\boldsymbol{z}}^{\mathrm{c}}}{c} = \tilde{t} + T^{\mathrm{c}}. \tag{2.59}$$

Then, we have:

$$W_{\mathrm{R}}(\boldsymbol{y},\boldsymbol{z}) = \int_{-\tau/2+|T^{\mathrm{c}}|}^{\tau/2-|T^{\mathrm{c}}|} e^{i\alpha(\tilde{t}-T^{\mathrm{c}})^2}e^{-i\alpha(\tilde{t}+T^{\mathrm{c}})^2}d\tilde{t} = \int_{-\tau^{\mathrm{c}}/2}^{\tau^{\mathrm{c}}/2} e^{-i\alpha 4\tilde{t}T^{\mathrm{c}}}d\tilde{t}, \tag{2.60}$$

where $\tau^{\mathrm{c}} \overset{\mathrm{def}}{=} \tau - 2|T^{\mathrm{c}}|$. Consequently,

$$\begin{aligned} W_{\mathrm{R}}(\boldsymbol{y},\boldsymbol{z}) &= -\frac{1}{4i\alpha T^{\mathrm{c}}}\left(e^{-2i\alpha\tau^{\mathrm{c}}T^{\mathrm{c}}} - e^{2i\alpha\tau^{\mathrm{c}}T^{\mathrm{c}}}\right) = \frac{\sin(2\alpha\tau^{\mathrm{c}}T^{\mathrm{c}})}{2\alpha T^{\mathrm{c}}} \\ &= \tau^{\mathrm{c}}\,\mathrm{sinc}(2\alpha\tau^{\mathrm{c}}T^{\mathrm{c}}) = \tau^{\mathrm{c}}\,\mathrm{sinc}\left(B\frac{\tau^{\mathrm{c}}}{\tau}\frac{R_{\boldsymbol{y}}^{\mathrm{c}} - R_{\boldsymbol{z}}^{\mathrm{c}}}{c}\right). \end{aligned} \tag{2.61}$$

The central maximum of the sinc(·) in formula (2.61) is attained at $R_{\boldsymbol{y}}^{\mathrm{c}} = R_{\boldsymbol{z}}^{\mathrm{c}}$. In this case, the argument of the sinc(·) is equal to zero. The other possibility for the argument to be equal to zero is $\tau^{\mathrm{c}} = 0 \;\Leftrightarrow\; |T^{\mathrm{c}}| = \tau/2$. It, however, should not be considered, because the overall function $\tau^{\mathrm{c}}\,\mathrm{sinc}(\,\cdot\,)$ does not have a maximum there (for the same reason as discussed in the beginning of Section 2.4.3). Moreover, we are primarily interested in the case $|T^{\mathrm{c}}| \ll \tau$. Indeed, $|T^{\mathrm{c}}|$ is the absolute value of the difference between the travel times from two close locations on the target, $\boldsymbol{y}$ and $\boldsymbol{z}$, to the radar antenna on the orbit, see Figure 2.1. If, however, we were to have $|T^{\mathrm{c}}| \sim \tau$, this would correspond to a large difference between $R_{\boldsymbol{y}}^{\mathrm{c}}$ and $R_{\boldsymbol{z}}^{\mathrm{c}}$, on the order of kilometers for the typical vales of the parameters from Table 1.1.

The first zero of the sinc(·) in (2.61) is attained when its argument is equal to π. To determine the location of the first zero, we have to solve the equation [cf. equation (2.54)]

$$B\Big(1-\frac{2T^{\mathrm{c}}}{\tau}\Big)T^{\mathrm{c}}=\pi, \tag{2.62}$$

where we have substituted $(R_y^{\mathrm{c}}-R_z^{\mathrm{c}})/c=T^{\mathrm{c}}$ and also replaced $|T^{\mathrm{c}}|$ with T^{c}, because the case $|T^{\mathrm{c}}|=-T^{\mathrm{c}}$ is analyzed similarly. The quadratic equation (2.62) has the roots [cf. formula (2.55)]:

$$\begin{aligned} T^{\mathrm{c}} &= \frac{\tau}{4B}\bigg(B\mp B\sqrt{1-\frac{8\pi}{B\tau}}\bigg)\\ &\approx \frac{\tau}{4B}\bigg(B\mp B\Big(1-\frac{4\pi}{B\tau}\Big)\bigg). \end{aligned} \tag{2.63}$$

Similarly to (2.55), we have employed the first order Taylor approximation of the square root on the first line of (2.63) because

$$\frac{8\pi}{B\tau}\ll 1.$$

Indeed, the compression ratio of the chirp, $B\tau/2\pi$, (i.e., its TBP) is always chosen to be large, see the typical value in Table 1.2.

The first root (2.63) is

$$T^{\mathrm{c}}=\frac{\pi}{B}\quad\Leftrightarrow\quad R_y^{\mathrm{c}}-R_z^{\mathrm{c}}=\frac{\pi c}{B}\stackrel{\mathrm{def}}{=}\Delta_{\mathrm{R}}. \tag{2.64}$$

It obviously satisfies the constraint $|T^{\mathrm{c}}|\ll\tau$ because again, the TBP of the chirp is large, $B\tau\gg 1$. The second root (2.63) is of no further interest:

$$T^{\mathrm{c}}=\frac{\tau}{2}-\frac{\pi}{B},$$

because for this root we have $|T^{\mathrm{c}}|\sim\tau$ rather than $|T^{\mathrm{c}}|\ll\tau$.

The main lobe of the sinc(·) in (2.61), if considered as a function of $R_y^{\mathrm{c}}-R_z^{\mathrm{c}}$, is located on the interval $[-\Delta_{\mathrm{R}},\Delta_{\mathrm{R}}]$. Inside this interval, we can replace τ^{c} by τ on the right-hand side of (2.61) and thus obtain [cf. formula (2.58)]:

$$W_{\mathrm{R}}(\boldsymbol{y},\boldsymbol{z})\approx\ \tau\,\mathrm{sinc}\left(\frac{B}{c}(R_y^{\mathrm{c}}-R_z^{\mathrm{c}})\right)=\tau\,\mathrm{sinc}\left(\pi\,\frac{R_y^{\mathrm{c}}-R_z^{\mathrm{c}}}{\Delta_{\mathrm{R}}}\right). \tag{2.65}$$

In doing so, we are also replacing τ^{c} by τ in front of the sinc(·), which only results in an insignificant change of the amplitude. Altogether, we conclude that the effect of T^{c} on the integration limits in (2.60) is small and can be disregarded.

2.4.5 Fourier interpretation of the data inversion

The fact that both $W_{\mathrm{A}}(\boldsymbol{y},\boldsymbol{z})$, see (2.58), and $W_{\mathrm{R}}(\boldsymbol{y},\boldsymbol{z})$, see (2.65), evaluate to a sinc function is not accidental. For the range factor $W_{\mathrm{R}}(\boldsymbol{y},\boldsymbol{z})$, the sinc comes as an implication of the linear variation of the instantaneous frequency (2.12) along the chirp: $\omega(t) = \omega_0 + \frac{B}{\tau}t$, where $t \in [-\tau/2, \tau/2]$, so that the integral (2.60) can be recast as

$$W_{\mathrm{R}}(\boldsymbol{y},\boldsymbol{z}) = \int_{-\tau^{\mathrm{c}}/2}^{\tau^{\mathrm{c}}/2} e^{-2i(\omega(\tilde{t})-\omega_0)T^{\mathrm{c}}} d\tilde{t}. \tag{2.66}$$

As for the azimuthal factor $W_{\mathrm{A}}(\boldsymbol{y},\boldsymbol{z})$, the exponents under the sum in (2.44) can be thought of as representing a linear variation of the local wavenumber along the synthetic array. Indeed, the quantity

$$k(\tilde{n}) \stackrel{\mathrm{def}}{=} \frac{k_0 L_{\mathrm{SA}} \tilde{n}}{RN} \tag{2.67}$$

depends linearly on $\tilde{n}$, and from (2.44) and (2.58) we have:

$$W_{\mathrm{A}}(\boldsymbol{y},\boldsymbol{z}) = \sum_{\tilde{n}=-\tilde{N}/2}^{\tilde{N}/2} e^{2ik(\tilde{n})(y_1-z_1)}, \tag{2.68}$$

which is very similar to (2.66), because $y_1 - z_1$ can substitute for $T^{\mathrm{c}} \propto (R^{\mathrm{c}}_{\boldsymbol{y}} - R^{\mathrm{c}}_{\boldsymbol{z}})$, and $k(\tilde{n})$ is a linear function of $\tilde{n}$ that turns into zero exactly in the middle of the summation interval, i.e., at $\tilde{n} = 0 \;\Leftrightarrow\; n = n_{\mathrm{c}}$, much like $\omega(\tilde{t}) - \omega_0$ turns into zero in the middle of the chirp (2.10). The difference between (2.66) and (2.68) is that the former is an integral and the latter is a sum, but a sum of type (2.68) can always be thought of as a quadrature formula of the Newton-Cotes type approximating the corresponding integral, see [15, Section 4.1].

Formulae (2.66) and (2.68) allow for an intuitive and convenient yet semi-qualitative Fourier interpretation of the SAR data inversion algorithm. Indeed, if we were to replace the integral on the right-hand side of (2.66) by an integral over the entire real axis, then the latter could be thought of as a genuine Fourier transform that evaluates to a δ-function (in the sense of distributions):

$$\int_{-\infty}^{\infty} e^{-4i\alpha\tilde{t}\left(\frac{R^{\mathrm{c}}_{\boldsymbol{y}}}{c}-\frac{R^{\mathrm{c}}_{\boldsymbol{z}}}{c}\right)} d\tilde{t} = \frac{\pi}{2\alpha}\delta\left(\frac{R^{\mathrm{c}}_{\boldsymbol{y}}}{c} - \frac{R^{\mathrm{c}}_{\boldsymbol{z}}}{c}\right).$$

An analogous interpretation that would result in $\delta(y_1 - z_1)$ can obviously be given to (2.68), with an additional caveat that it is a sum rather than an integral. Substituting the δ-functions instead of W_{R} and W_{A} would make the data inversion exact. Hence, it is the discrepancy between the right-hand sides of (2.66) and (2.68) and the corresponding true Fourier transforms that explains the approximate nature of the foregoing SAR data inversion algorithm. A similar Fourier-based treatment of the matched filter (2.23) is given in Appendix 2.A.

2.4.6 Doppler viewpoint for the azimuthal reconstruction

The "instantaneous" wavenumber $k(\tilde{n})$ of (2.67) can be recast as follows:

$$\begin{aligned} k(\tilde{n}) &= \frac{k_0}{R}\Big(\frac{L_{\mathrm{SA}}n}{N} - \frac{L_{\mathrm{SA}}n_{\mathrm{c}}}{N}\Big) \approx k_0\frac{x_1^n - (y_1+z_1)/2}{R} \\ &= \frac{k_0}{2}\Big[\frac{x_1^n - y_1}{R} + \frac{x_1^n - z_1}{R}\Big] = -\frac{k_0}{2}\Big[\tan\Big(\frac{\pi}{2} - \gamma_y^n\Big) + \tan\Big(\frac{\pi}{2} - \gamma_z^n\Big)\Big] \\ &\approx -\frac{k_0}{2}\Big[\sin\Big(\frac{\pi}{2} - \gamma_y^n\Big) + \sin\Big(\frac{\pi}{2} - \gamma_z^n\Big)\Big] \\ &\approx -k_0\sin\Big(\frac{\pi}{2} - \frac{\gamma_y^n + \gamma_z^n}{2}\Big) = -k_0\cos\frac{\gamma_y^n + \gamma_z^n}{2} \stackrel{\mathrm{def}}{=} -k_0\cos\tilde{\gamma}^n, \end{aligned} \tag{2.69}$$

where $\tilde{n}$ and n are related by (2.43), and γ_y^n and γ_z^n are the angles between the platform velocity and the direction from $\boldsymbol{x}^n$ to $\boldsymbol{y}$ and to $\boldsymbol{z}$, respectively, see Figure 2.1. Note that for narrow antenna beams and broadside imaging, the angles $\frac{\pi}{2} - \gamma_y^n$ and $\frac{\pi}{2} - \gamma_z^n$ are small; that's why the approximation in (2.69) holds. Using (2.69) we can recast (2.68) as

$$W_{\mathrm{A}}(\boldsymbol{y},\boldsymbol{z}) \approx \sum_{n=n_{\mathrm{c}}-\tilde{N}/2}^{n_{\mathrm{c}}+\tilde{N}/2} e^{-2ik_0\cos\tilde{\gamma}^n(y_1-z_1)} = \sum_{n=n_{\mathrm{c}}-\tilde{N}/2}^{n_{\mathrm{c}}+\tilde{N}/2} e^{-2i\omega_0\cos\tilde{\gamma}^n(y_1-z_1)/c}, \tag{2.70}$$

which shows that the variation of the local wavenumber along the synthetic array can be attributed to a Doppler-like effect. Indeed, it is well-known that the standard linear Doppler frequency shift (for more detail, see Section 6.1 and, specifically, equation (6.7b)) is proportional to the ratio of the platform speed $\mathfrak{v}$ to the wave propagation speed c (the velocity factor) times the cosine of the angle between the platform velocity and the direction to the target (the geometric factor):

$$\omega - \omega_0 \propto \frac{\mathfrak{v}}{c}\cos\gamma.$$

In formula (2.70), the actual physical Doppler effect, which is due to the platform motion, does not manifest itself, because we are using the start-stop approximation, and the platform is considered motionless at the times when it emits and receives the SAR signals.[6] On the other hand, as we have mentioned in Section 2.3.2, it is common to associate the change in the antenna position, i.e., the variation of n, with the so-called slow time. Then, the local wavenumber $k(n)$ given by the final expression in (2.69), $k(n) \stackrel{\mathrm{def}}{=} -k_0\cos\tilde{\gamma}^n$, can be thought of as a function of slow time. The dependence of $k(n)$ on slow time in (2.70) is through $\cos\tilde{\gamma}^n$, so that

[6] The role of the platform motion and the corresponding physical Doppler effect in SAR analysis is discussed in detail in Chapter 6.

its value is determined by the transmitting/receiving location n only and is not affected by how rapidly the platform moves between different locations. Thus, the quantity $\cos\tilde{\gamma}^n$ and hence the exponent in formula (2.70) can be interpreted as the second, geometric, contributing factor to the Doppler frequency shift in slow time. This frequency (rather, wavenumber) shift varies linearly along the synthetic array, see (2.67), which can also be seen as a chirp of length L_{SA} in the azimuthal direction. It is to be noted though that in the literature the Doppler interpretation of synthetic arrays is sometimes incorrectly attributed to the physical fast time t, as opposed to the slow time n, see, e.g., [79, Section 4.5.1] or [40, Section 1.4.2.2].

We note that formula (2.58) was obtained for the maximum length of the synthetic aperture that corresponds to the full width of the antenna beam, see (2.29). If the length of the synthetic aperture L_{SA} is taken smaller than that, then $W_\Sigma(\boldsymbol{y},\boldsymbol{z})$ of (2.58) acquires an insignificant phase multiplier that depends on the azimuthal coordinate (an equivalent analysis for the imaging in range can be found in [79, Section 3A.2]).

Let us additionally recall that formula (2.40) was derived with the help of linearization (i.e., first order Taylor expansion) of the square roots in (2.38) and (2.39). One can also obtain the next term in the expansion assuming that L_{SA}/R is a small parameter. Then, using (2.43) and taking into account that $|l| \ll R$ and $|y_1 - z_1| \ll R$, we can write:

$$R_y^n - R_z^n \approx \frac{Ll}{R} - \frac{y_1 - z_1}{R}(\tilde{n}\Delta x_1) - \frac{Ll}{2R^3}(\tilde{n}\Delta x_1)^2. \tag{2.71}$$

If the last term on the right-hand side of (2.71), which is quadratic with respect to $\tilde{n}$, is included into the exponents under the sum in (2.44), then those exponents will not all turn into zero for any choice of y_1 unless $l = 0$, i.e., unless $y_2 = z_2$. This can be thought of as a quadratic phase error (QPE) between the signal and the matched filter. One of its implications for imaging is a slight smearing of the sinc shape in (2.58) for $l \neq 0$. We will, however, postpone the discussion of QPE until Chapter 3, see formula (3.122), where this error is independent of the range coordinate and comes from the propagation of radar signals in a dispersive medium rather than from the geometry, as in (2.71).

In the next section, we estimate the error associated with the approximate factorized representation (2.34) of the GAF $W(\boldsymbol{y},\boldsymbol{z})$.

2.5 Factorization error of the GAF

The approach we follow in this section for evaluating the integrals involved in the GAF is similar to that of Section 2.4. First, we take into account (2.42) and recast the genuine non-factorized expression (2.32) for the GAF as follows:

$$
\begin{aligned}
W(\boldsymbol{y},\boldsymbol{z}) &= \sum_{n=N_1(\boldsymbol{y},\boldsymbol{z})}^{N_2(\boldsymbol{y},\boldsymbol{z})} \int_{\chi} \overline{A(t-2R_{\boldsymbol{y}}^n/c)} A(t-2R_{\boldsymbol{z}}^n/c) e^{2i\omega_0(R_{\boldsymbol{z}}^n/c - R_{\boldsymbol{y}}^n/c)} dt \\
&= \sum_{n=N_1(\boldsymbol{y},\boldsymbol{z})}^{N_2(\boldsymbol{y},\boldsymbol{z})} \int_{\chi} \chi_\tau(t-t_{\boldsymbol{y}}^n) e^{i\alpha(t-t_{\boldsymbol{y}}^n)^2} \chi_\tau(t-t_{\boldsymbol{z}}^n) e^{-i\alpha(t-t_{\boldsymbol{z}}^n)^2} \\
&\qquad\qquad \cdot e^{i\omega_0(t_{\boldsymbol{z}}^n - t_{\boldsymbol{y}}^n)} dt,
\end{aligned}
\tag{2.72}
$$

where the integration variable has been changed as suggested in the beginning of Section 2.4: : $t - t_n \mapsto t$, and new notations have been used:

$$
t_{\boldsymbol{y}}^n \stackrel{\text{def}}{=} \frac{2R_{\boldsymbol{y}}^n}{c} = \frac{2|\boldsymbol{x}^n - \boldsymbol{y}|}{c} \text{ and } t_{\boldsymbol{z}}^n \stackrel{\text{def}}{=} \frac{2R_{\boldsymbol{z}}^n}{c} = \frac{2|\boldsymbol{x}^n - \boldsymbol{z}|}{c}. \tag{2.73}
$$

Then, similarly to (2.59), we introduce a new integration variable $\tilde{t}$ and new constants T^n:

$$
\tilde{t} = t - \frac{t_{\boldsymbol{z}}^n + t_{\boldsymbol{y}}^n}{2}, \quad T^n = \frac{t_{\boldsymbol{y}}^n - t_{\boldsymbol{z}}^n}{2} \equiv \frac{R_{\boldsymbol{y}}^n - R_{\boldsymbol{z}}^n}{c}, \tag{2.74}
$$

so that

$$
t - t_{\boldsymbol{y}}^n = \tilde{t} - T^n \text{ and } t - t_{\boldsymbol{z}}^n = \tilde{t} + T^n.
$$

As mentioned in Section 2.4.1 (see the discussion right after equation (2.61)), a typical travel time between $\boldsymbol{y}$ and $\boldsymbol{z}$ is much shorter than the duration of the pulse. This is equivalent to $|T^n| \ll \tau$; hence, the two indicator functions χ_τ under the integral in (2.72) overlap on some interval.[7] The center of this interval is $\tilde{t} = 0$ and the endpoints are $\tilde{t} = \tau/2 - |T^n|$ and $\tilde{t} = -\tau/2 + |T^n|$, so that its length is

$$
\tau^n = \tau - 2|T^n|. \tag{2.75}
$$

The phase of the integrand in (2.72) can be expressed as

$$
\begin{aligned}
&\alpha(t-t_{\boldsymbol{y}}^n)^2 - \alpha(t-t_{\boldsymbol{z}}^n)^2 + \omega_0(t_{\boldsymbol{z}}^n - t_{\boldsymbol{y}}^n) \\
&= \alpha\Big((\tilde{t}-T^n)^2 - (\tilde{t}+T^n)^2\Big) + \omega_0(t-(\tilde{t}+T^n) - (t-(\tilde{t}-T^n))) \\
&= -\alpha \cdot 4\tilde{t}T^n - 2\omega_0 T^n,
\end{aligned}
$$

[7] That's why, unlike in (2.41), we do not have $\chi_{2L_{\text{SA}}}(y_1 - z_1)$ in front of the sum in (2.72).

so the integration can be carried out analytically [cf. formula (2.60)]:

$$\begin{aligned} W(\boldsymbol{y},\boldsymbol{z}) &= \sum_{n=N_1(\boldsymbol{y},\boldsymbol{z})}^{N_2(\boldsymbol{y},\boldsymbol{z})} e^{-2i\omega_0 T^n} \int_{-\tau^n/2}^{\tau^n/2} e^{-4i\alpha T^n \tilde{t}}\, d\tilde{t} \\ &= \sum_{n=N_1(\boldsymbol{y},\boldsymbol{z})}^{N_2(\boldsymbol{y},\boldsymbol{z})} e^{-2i\omega_0 T^n} \frac{-1}{4i\alpha T^n} (e^{-2i\alpha\tau^n T^n} - e^{2i\alpha\tau^n T^n}) \\ &= \sum_{n=N_1(\boldsymbol{y},\boldsymbol{z})}^{N_2(\boldsymbol{y},\boldsymbol{z})} e^{-2i\omega_0 T^n} \frac{1}{4i\alpha T^n} 2i \sin(2\alpha\tau^n T^n) \\ &= \sum_{n=N_1(\boldsymbol{y},\boldsymbol{z})}^{N_2(\boldsymbol{y},\boldsymbol{z})} e^{-2i\omega_0 T^n} \tau^n \operatorname{sinc}(2\alpha\tau^n T^n). \end{aligned} \tag{2.76}$$

Let us now introduce a new function:

$$W_{(\mathrm{R}\Sigma)}(\boldsymbol{y},\boldsymbol{z}) \stackrel{\text{def}}{=} W_{\mathrm{R}}(\boldsymbol{y},\boldsymbol{z}) \cdot W_{\Sigma}(\boldsymbol{y},\boldsymbol{z}), \tag{2.77}$$

where similarly to (2.41),

$$W_{\Sigma}(\boldsymbol{y},\boldsymbol{z}) = \sum_{n=N_1(\boldsymbol{y},\boldsymbol{z})}^{N_2(\boldsymbol{y},\boldsymbol{z})} e^{2i\omega_0 (R_z^n - R_y^n)/c} = \sum_{n=N_1(\boldsymbol{y},\boldsymbol{z})}^{N_2(\boldsymbol{y},\boldsymbol{z})} e^{-2i\omega_0 T^n},$$

and similarly to (2.36),

$$W_{\mathrm{R}}(\boldsymbol{y},\boldsymbol{z}) = \int_{\chi} \overline{A(t - 2R_y^{\mathrm{c}}/c)} A(t - 2R_z^{\mathrm{c}}/c)\, dt = \tau^{\mathrm{c}} \operatorname{sinc}(2\alpha\tau^{\mathrm{c}} T^{\mathrm{c}}). \tag{2.78}$$

In formula (2.78), τ^{c} and T^{c} denote τ^n and T^n, respectively, for $n = n_{\mathrm{c}}$, see (2.43), and are, of course, the same as τ^{c} and T^{c} of Section 2.4. We emphasize that unlike the approximation (2.34), formula (2.77) is the exact definition of a new function. Our goal is to determine how accurately this new function $W_{(\mathrm{R}\Sigma)}(\boldsymbol{y},\boldsymbol{z})$ of (2.77)–(2.78) approximates the GAF $W(\boldsymbol{y},\boldsymbol{z})$ of (2.72) or, equivalently, (2.76). To assess the accuracy of approximation, we will estimate the error

$$W - W_{(\mathrm{R}\Sigma)} = \sum_{n=N_1(\boldsymbol{y},\boldsymbol{z})}^{N_2(\boldsymbol{y},\boldsymbol{z})} e^{-2i\omega_0 T^n} [\tau^n \operatorname{sinc}(2\alpha\tau^n T^n) - \tau^{\mathrm{c}} \operatorname{sinc}(2\alpha\tau^{\mathrm{c}} T^{\mathrm{c}})]. \tag{2.79}$$

Using (2.40), (2.43), and (2.74), taking into account that $x_1^n = n\Delta x_1 = nL_{\mathrm{SA}}/N$, and recalling that $L/R = \sin\theta$, we can write:

$$\begin{aligned} T^n &= \frac{R_y^n - R_z^n}{c} = \frac{Ll}{Rc} + \frac{l^2\cos^2\theta}{2Rc} - \frac{z_1^2 - y_1^2}{2Rc} - \frac{(y_1 - z_1)x_1^n}{Rc} \\ &\approx \frac{l\sin\theta}{c} - \frac{y_1 - z_1}{c}\Big(\frac{x_1^n}{R} - \frac{y_1 + z_1}{2R}\Big) \\ &= \frac{l\sin\theta}{c} - \frac{y_1 - z_1}{c}\frac{L_{\mathrm{SA}}}{RN}\tilde{n} \stackrel{\mathrm{def}}{=} T^{\mathrm{c}} - \mathcal{T}^{\tilde{n}}, \end{aligned} \tag{2.80}$$

where

$$\mathcal{T}^{\tilde{n}} = \frac{(y_1 - z_1)L_{\mathrm{SA}}}{NcR}\tilde{n} \stackrel{\mathrm{def}}{=} \tilde{n}\mathcal{T}^1 \quad \text{and} \quad \mathcal{T}^1 = \frac{(y_1 - z_1)L_{\mathrm{SA}}}{NcR}. \tag{2.81}$$

Using (2.43), we change the summation variable in (2.79) from n to $\tilde{n}$:

$$W - W_{(\mathrm{R}\Sigma)} = \sum_{\tilde{n}=-\tilde{N}/2}^{\tilde{N}/2} e^{-2i\omega_0 T^{\tilde{n}}}[\tau^{\tilde{n}}\,\mathrm{sinc}(2\alpha\tau^{\tilde{n}}T^{\tilde{n}}) - \tau^{\mathrm{c}}\,\mathrm{sinc}(2\alpha\tau^{\mathrm{c}}T^{\mathrm{c}})], \tag{2.82}$$

where [cf. formulae (2.74) and (2.75)]

$$T^{\tilde{n}} = T^{\mathrm{c}} - \mathcal{T}^{\tilde{n}} \quad \text{and} \quad \tau^{\tilde{n}} = \tau - 2|T^{\tilde{n}}|.$$

As $|T^{\mathrm{c}}| \ll \tau$ and $|\mathcal{T}^{\tilde{n}}| \ll \tau$, we can write using the first order Taylor formula:

$$\begin{aligned} \mathrm{sinc}(2\alpha\tau^{\tilde{n}}T^{\tilde{n}}) &\approx \mathrm{sinc}(2\alpha\tau^{\mathrm{c}}T^{\mathrm{c}}) + 2\alpha(\tau^{\tilde{n}}T^{\tilde{n}} - \tau^{\mathrm{c}}T^{\mathrm{c}})\,\mathrm{sinc}'(2\alpha\tau^{\mathrm{c}}T^{\mathrm{c}}) \\ &\approx \mathrm{sinc}(2\alpha\tau^{\mathrm{c}}T^{\mathrm{c}}) - 2\alpha\tau\mathcal{T}^{\tilde{n}}\,\mathrm{sinc}'(2\alpha\tau^{\mathrm{c}}T^{\mathrm{c}}), \end{aligned} \tag{2.83}$$

where in the increment of the argument $(\tau^{\tilde{n}}T^{\tilde{n}} - \tau^{\mathrm{c}}T^{\mathrm{c}})$ we have disregarded all the terms higher than first order with respect to either T^{c} or $\mathcal{T}^{\tilde{n}}$. With the help of (2.83), the expression in square brackets on the right-hand side of (2.79) evaluates to

$$\begin{aligned} &\tau^{\tilde{n}}\,\mathrm{sinc}(2\alpha\tau^{\tilde{n}}T^{\tilde{n}}) - \tau^{\mathrm{c}}\,\mathrm{sinc}(2\alpha\tau^{\mathrm{c}}T^{\mathrm{c}}) \\ &\approx 2(|T^{\mathrm{c}}| - |T^{\tilde{n}}|)\,\mathrm{sinc}(2\alpha\tau^{\mathrm{c}}T^{\mathrm{c}}) - 2\alpha\tau^2\mathcal{T}^{\tilde{n}}\,\mathrm{sinc}'(2\alpha\tau^{\mathrm{c}}T^{\mathrm{c}}), \end{aligned} \tag{2.84}$$

where again, we have neglected all the terms higher than first order with respect to either T^{c} or $\mathcal{T}^{\tilde{n}}$. Moreover, as $\alpha\tau^2 = B\tau/2 \gg 1$ (the TBP of the chirp $\frac{B\tau}{2\pi}$ is considered large, see Table 1.2), the second term on the right-hand side of the previous equality appears much greater than the first term (taking into account that $|\,\mathrm{sinc}'(2\alpha\tau^{\mathrm{c}}T^{\mathrm{c}})| < \frac{1}{2}$). Then, dropping the first term and denoting

$$S = -2\alpha\tau^2\,\mathrm{sinc}'(2\alpha\tau^{\mathrm{c}}T^{\mathrm{c}}), \tag{2.85}$$

we can transform formula (2.82) into

$$W - W_{(\mathrm{R}\Sigma)} \approx e^{i\Phi_0} S \sum_{\tilde{n}=-\tilde{N}/2}^{\tilde{N}/2} e^{2i\omega_0 \mathcal{T}^{\tilde{n}}} \mathcal{T}^{\tilde{n}} = S\mathcal{T}^1 e^{i\Phi_0} \sum_{\tilde{n}=-\tilde{N}/2}^{\tilde{N}/2} \tilde{n} e^{i\tilde{n}\varphi}, \tag{2.86}$$

where according to (2.80) and (2.81) we have [cf. formula (2.46)]:

$$\Phi_0 = -2\frac{\omega_0 l}{c}\sin\theta \ \text{ and } \ \varphi = 2\omega_0 \mathcal{T}^1 = 2\frac{\omega_0 L_{\mathrm{SA}}}{NRc}(y_1 - z_1). \tag{2.87}$$

To calculate the sum on the right-hand side of (2.86), we differentiate the left-hand side and the right-hand side of (2.52) with respect to φ:

$$\sum_{\tilde{n}=-\tilde{N}/2}^{\tilde{N}/2} \tilde{n} e^{in\varphi} = \frac{1}{i}\frac{\partial}{\partial\varphi} \sum_{\tilde{n}=-\tilde{N}/2}^{\tilde{N}/2} e^{in\varphi} \approx \frac{1}{i}\frac{\partial}{\partial\varphi}\Big(\tilde{N}\,\mathrm{sinc}\,\frac{\tilde{N}\varphi}{2}\Big) = \frac{\tilde{N}^2}{2i}\,\mathrm{sinc}'\,\frac{\tilde{N}\varphi}{2}.$$

Then, similarly to Section 2.4.1, we replace $\tilde{N}$ with N and using (2.85), obtain the following expression for the factorization error (2.86):

$$W - W_{(\mathrm{R}\Sigma)} \approx S\mathcal{T}^1 \frac{N^2}{2i} e^{i\Phi_0}\,\mathrm{sinc}'\,\frac{N\varphi}{2} = \frac{NS}{2i\omega_0} e^{i\Phi_0}\frac{N\varphi}{2}\,\mathrm{sinc}'\,\frac{N\varphi}{2}, \tag{2.88}$$

where according to (2.57) and (2.87):

$$\frac{N\varphi}{2} = \frac{\pi(y_1 - z_1)}{\Delta_{\mathrm{A}}}. \tag{2.89}$$

Hence, for the relative error of factorization we can write using (2.88) along with (2.65) and (2.58):

$$\frac{\max|W - W_{(\mathrm{R}\Sigma)}|}{\max|W_{(\mathrm{R}\Sigma)}|} = \frac{1}{N\tau}\frac{N|S|}{2\omega_0}\Big|\frac{N\varphi}{2}\Big|\,\Big|\,\mathrm{sinc}'\,\frac{N\varphi}{2}\Big|. \tag{2.90}$$

Note that both W and $W_{(\mathrm{R}\Sigma)}$ are complex-valued quantities. Hence, keeping the absolute value of their difference small is necessary and sufficient for these two quantities to be close to one another. That, in turn, allows one to use the factorized GAF $W_{(\mathrm{R}\Sigma)}$, which is easier to analyze, for assessing the quality of the original non-factorized GAF W.

To obtain an estimate for the right-hand side of equation (2.90) we first notice that

$$\max_{x\in(-\infty,\infty)} |\,\mathrm{sinc}'(x)| < \frac{1}{2}.$$

Then, given the definition of S by formula (2.85) and taking into account (2.89), we have:

$$\frac{\max|W - W_{(\mathrm{R}\Sigma)}|}{\max|W_{(\mathrm{R}\Sigma)}|} < \frac{\alpha\tau}{4\omega_0}\frac{\pi|y_1 - z_1|}{\Delta_{\mathrm{A}}} = \frac{B}{8\omega_0}\frac{\pi|y_1 - z_1|}{\Delta_{\mathrm{A}}}. \tag{2.91}$$

Hereafter, we will only be interested in considering $|y_1 - z_1| \lesssim \Delta_{\mathrm{A}}$ or, equivalently, considering only the main lobe of the $\mathrm{sinc}(\,\cdot\,)$ in the azimuthal factor (2.58), see Section 2.6 for further details. Then, from (2.91) we obtain:

$$\frac{\max|W - W_{(\mathrm{R}\Sigma)}|}{\max|W_{(\mathrm{R}\Sigma)}|} \lesssim \frac{\pi}{8}\frac{B}{\omega_0}. \tag{2.92}$$

Formula (2.92) provides an estimate for the relative error due to the factorization (2.77)–(2.78) or, equivalently, (2.34)–(2.36). This error is on the order of one percent, given the value of the relative bandwidth $\frac{B}{\omega_0} \approx 3 \cdot 10^{-2}$ presented in Table 1.2. It is interesting to note that according to (2.88), the dominant term of this error vanishes if either $y_1 = z_1$ or $y_2 = z_2$ (the latter implies $T^{\mathrm{c}} = 0$, see (2.81), and hence $S = 0$, see (2.85)). The key to understanding this effect is the expression for $T^{\tilde{n}}$ in (2.80)–(2.82). Physically, $T^{\tilde{n}}$ is the difference between the pulse two-way travel time for the pairs $(\boldsymbol{x}^n, \boldsymbol{y})$ and $(\boldsymbol{x}^n, \boldsymbol{z})$. As a function of the satellite position n, $T^{\tilde{n}}$ has a constant part T^{c} and a part $\mathcal{T}^{\tilde{n}}$ which is linear in $\tilde{n} = n - n_{\mathrm{c}}$. It is the variation of the range PSF $\mathrm{sinc}(2\alpha\tau^{\tilde{n}}T^{\tilde{n}})$ with $\tilde{n}$ in formula (2.82) that is responsible for the leading term of the factorization error. If $y_2 = z_2$, then the constant part of $T^{\tilde{n}}$ vanishes and so does the PSF tangent slope given by $\mathrm{sinc}'(2\alpha\tau^{\mathrm{c}}T^{\mathrm{c}})$. Hence, the leading term of the variation of the PSF disappears. On the other hand, if $y_1 = z_1$ then it is the leading term of the variation of $T^{\tilde{n}}$ with $\tilde{n}$ that vanishes ($\mathcal{T}^{\tilde{n}} \equiv 0$, see (2.81)), and so does the leading term of the variation of $\mathrm{sinc}(2\alpha\tau^{\tilde{n}}T^{\tilde{n}})$ regardless of the value of $2\alpha\tau^{\mathrm{c}}T^{\mathrm{c}}$. Only in the general "diagonal" configuration: $y_1 \neq z_1$ and $y_2 \neq z_2$, does the coupling between the range and azimuthal terms become significant, which yields the full unabridged expression for the error (2.88).

2.6 Resolution

A key measure of radar performance is its capacity to tell between two closely located point targets. It is called the resolution, and it directly affects the quality of the image. The generalized ambiguity function built in Section 2.4 provides a very efficient tool for studying the SAR resolution because it can be conveniently interpreted as the image of a point target. Moreover, the factorized form of the GAF (2.34) proves very useful in that it allows one to quantify the performance of the SAR sensor independently in different directions.

First of all, we notice that according to formulae (2.35), (2.36), (2.65), and (2.58) the factorized GAF (2.34) is a function of only two independent spatial directions — the azimuthal direction which is parallel to the flight track and the slant

range direction which is normal to the flight track. On one hand, this basically means that the SAR data collection algorithm we have described (a monostatic non-interferometric sensor traveling along a linear trajectory) can generate only two-dimensional datasets, and we expect that it will provide resolution only in those two directions (range and azimuth). On the other hand, it leads to a certain vagueness because $\nu(\boldsymbol{z})$ is a function of three variables and the integration in (2.31) (and prior to that, in (2.22)) is performed over a 3D region ($\boldsymbol{z} \in \mathbb{R}^3$). A standard way of removing this vagueness in the SAR ambiguity theory [9, 75, 86] consists of artificially restricting the dimension of the set on which $\nu(\boldsymbol{z})$ is specified. This is done by eliminating the vertical coordinate and defining the plane $z_3 = 0$, i.e., the surface of the Earth, as the locus of all the targets. Accordingly, the ground reflectivity function (2.15′) becomes

$$\nu(\boldsymbol{z}) \equiv \nu(z_1, z_2, z_3) = \nu(z_1, z_2)\delta(z_3), \tag{2.93}$$

which is a single layer, or layer of monopoles, on the surface. From the standpoint of physics, considering the reflectivity in the form of (2.93) merely suggests that all the scattering occurs only at the surface of the target, which is what one intuitively expects when imaging the Earth from an aircraft or a satellite. The integration in (2.31) is then performed over a 2D region (plane), and the resulting image reconstructs $\nu(z_1, z_2)$, i.e., yields the reflectivity on the surface of the Earth as a function of the two horizontal coordinates.

To analyze the performance of the SAR instrument in the azimuthal and range directions, we use the individual factors of the GAF $W_\Sigma(\boldsymbol{y}, \boldsymbol{z})$ and $W_\mathrm{R}(\boldsymbol{y}, \boldsymbol{z})$ given by formulae (2.58) and (2.65), respectively. Introducing the same notation as in the first equality of (2.87):

$$\Phi_0 = -2k_0 \frac{Ll}{R},$$

we can recast (2.58) as

$$W_\Sigma(\boldsymbol{y}, \boldsymbol{z}) \approx e^{i\Phi_0} W_\mathrm{A}(\boldsymbol{y}, \boldsymbol{z}), \tag{2.94}$$

where [cf. (2.57)]

$$W_\mathrm{A}(\boldsymbol{y}, \boldsymbol{z}) = N \operatorname{sinc}\left(\pi \frac{y_1 - z_1}{\Delta_\mathrm{A}}\right) \quad \text{and} \quad \Delta_\mathrm{A} = \frac{\pi R c}{\omega_0 L_\mathrm{SA}}. \tag{2.95}$$

The sinc function in (2.95) attains its maximum at $y_1 = z_1$ and has its first zero where $y_1 - z_1 = \Delta_\mathrm{A}$. Therefore, Δ_A is the semi-width of the main lobe of the $\operatorname{sinc}(\cdot)$. The quantity Δ_A given by the second equality of (2.95) (and also by (2.57)) is called the azimuthal resolution, because it is assumed that if two point targets are at least Δ_A apart, then their images given by sinc functions of semi-width Δ_A can be distinguished from one another. For the typical values of the parameters given in Table 1.1, the azimuthal resolution Δ_A of (2.95) evaluates to approximately $10m$. Altogether, the function $W_\mathrm{A}(\boldsymbol{y}, \boldsymbol{z})$ of (2.95) describes the performance of the SAR sensor in the azimuthal direction.

For the second factor, W_{R}, we can write in accordance with (2.64), (2.65):

$$W_{\mathrm{R}}(\boldsymbol{y},\boldsymbol{z}) \approx \tau\,\mathrm{sinc}\left(\pi\frac{R_{\boldsymbol{y}}^{\mathrm{c}}-R_{\boldsymbol{z}}^{\mathrm{c}}}{\Delta_{\mathrm{R}}}\right),\quad \text{where}\quad \Delta_{\mathrm{R}}=\frac{\pi c}{B}. \tag{2.96}$$

The exact same argument as in the case of azimuthal resolution allows one to interpret the quantity Δ_{R} in formula (2.96), see also (2.64), as the range resolution. The function $W_{\mathrm{R}}(\boldsymbol{y},\boldsymbol{z})$ describes the performance of the SAR sensor in the range direction. Moreover, we see that the range resolution Δ_{R} is about $B\tau$ times smaller than the plain spatial length of the chirp $c\tau$. That's why the TBP of the chirp $\frac{B\tau}{2\pi}$ is also called its compression ratio. For the chirp bandwidth B defined in Table 1.1, the numerical value of the range resolution Δ_{R} defined in formula (2.96) is approximately $19m$.

Given the idea behind the definition of the compression ratio of the chirp, one can introduce a similar concept for the azimuthal direction as well. Indeed, according to the analysis of Section 2.4.6, the linear variation of the local wavenumber $k=k(\tilde{n})$ along the synthetic array can be interpreted as a chirp of length L_{SA}. Its ratio to the azimuthal resolution Δ_{A} (i.e., compression ratio):

$$\frac{L_{\mathrm{SA}}}{\Delta_{\mathrm{A}}}=\frac{2L_{\mathrm{SA}}^2}{\lambda_0}\frac{1}{R}\gg 1$$

is equal to the ratio of the Fraunhofer distance for the synthetic array over the distance from the antenna to the target, which is large, see Table 1.2.

Let us also recall that $n=n_{\mathrm{c}}$ of (2.43) corresponds to the center of the synthetic aperture when computing the imaging kernel. Hence, we can write: $x_1^{n_{\mathrm{c}}}=\frac{y_1+z_1}{2}$, and then formula (2.40) yields:

$$R_{\boldsymbol{y}}^{\mathrm{c}}-R_{\boldsymbol{z}}^{\mathrm{c}}\approx\frac{Ll}{R}+\frac{l^2\cos^2\theta}{2R}.$$

As $l=y_2-z_2$ and $|l|\ll R$, the second term on the right-hand side of the previous equality is much smaller than the first term and can be dropped. Hence, from the first equality of (2.96) we have:

$$W_{\mathrm{R}}(\boldsymbol{y},\boldsymbol{z})\approx\tau\,\mathrm{sinc}\left(\pi\frac{y_2-z_2}{\Delta_{\mathrm{R}}}\sin\theta\right). \tag{2.96$'$}$$

The difference between formulae (2.96) and (2.96$'$) is that the former shows the dependence of $W_{\mathrm{R}}(\boldsymbol{y},\boldsymbol{z})$ on the slant range variables $R_{\boldsymbol{y}}^{\mathrm{c}}$ and $R_{\boldsymbol{z}}^{\mathrm{c}}$, whereas the latter shows the dependence of $W_{\mathrm{R}}(\boldsymbol{y},\boldsymbol{z})$ on the actual range coordinates y_2 and z_2, see Figure 2.1. Accordingly, the resolution Δ_{R} defined in (2.96) is, in fact, the slant range resolution, while the actual range resolution derived from (2.96$'$) would be $\Delta_{\mathrm{R}}/\sin\theta$. However, the difference between the two is only by a constant factor of $1/\sin\theta$. Hence, throughout the book we will be using expressions of the type (2.96), as opposed to (2.96$'$), for assessing the performance of the SAR instrument in the range direction, and will be referring to Δ_{R} as the range resolution.

The overall expression for the factorized GAF $W(\boldsymbol{y}, \boldsymbol{z})$ of (2.34) becomes

$$W(\boldsymbol{y}, \boldsymbol{z}) = W_\Sigma(\boldsymbol{y}, \boldsymbol{z}) W_\mathrm{R}(\boldsymbol{y}, \boldsymbol{z}) = e^{i\Phi_0} W_\mathrm{A}(\boldsymbol{y}, \boldsymbol{z}) W_\mathrm{R}(\boldsymbol{y}, \boldsymbol{z}). \tag{2.97}$$

We notice that according to (2.40) and (2.94)–(2.96), the GAF depends only on the difference of its arguments: $W(\boldsymbol{y}, \boldsymbol{z}) = W(\boldsymbol{y} - \boldsymbol{z})$, which indeed allows us to interpret formula (2.31) with the kernel (2.34) as a convolution integral:

$$I(\boldsymbol{y}) = \int W(\boldsymbol{y}, \boldsymbol{z}) \nu(\boldsymbol{z}) d\boldsymbol{z} = \int W(\boldsymbol{y} - \boldsymbol{z}) \nu(\boldsymbol{z}) d\boldsymbol{z} = W * \nu.$$

Each of the two factors, W_A and W_R, describes the spreading of the GAF in the corresponding direction, i.e., a measure of how different it is from the ideal δ-function. We therefore conclude that the shape of the GAF $W(\boldsymbol{y}, \boldsymbol{z})$ directly affects the quality of the reconstruction of $\nu(\boldsymbol{z})$ in the form of $I(\boldsymbol{y})$, see (2.31).

We emphasize, however, that while the entire previous discussion in this section is based on the approximate factorized form of the GAF (2.34), the true GAF given by formula (2.32) is not factorized. As such, it does not provide a convenient form for studying, or even defining, the radar resolution independently for the range and azimuthal directions. That's why the factorization error that we computed in Section 2.5 becomes important — it quantifies the difference between the two forms of the GAF, the one that allows for a direct analysis of the SAR resolution and the one that does not. According to the estimate (2.92), the relative error of the GAF factorization is small, on the order of the relative bandwidth of the SAR system. Therefore, the approximate resolution analysis of this section that is based on the factorized form of the GAF (2.34) still provides an accurate assessment of the SAR performance. The factorization error in this context can be thought of as a source of image distortions, understood as discrepancies between the simplified factorized imaging kernel and its genuine non-factorized counterpart. Again, estimate (2.92) indicates that the relative magnitude of those distortions is not large for those parameters that we have chosen. Of course, for wide-band interrogating waveforms it may be substantial.

2.7 Deficiencies of the conventional approach

Earlier publications in the literature discussing the SAR ambiguity theory, including some of our own papers [1, 3, 5], did not distinguish between $W_\Sigma(\boldsymbol{y}, \boldsymbol{z})$ and $W_\mathrm{A}(\boldsymbol{y}, \boldsymbol{z})$, whereas these two factors are related by the fast phase multiplier $e^{i\Phi_0}$, see (2.87) and (2.94). As the absolute value of this multiplier is one, ignoring it has no effect on the expressions for resolution in either direction. That is why in the case of a point scatterer one can obtain the correct expressions for both the range and azimuthal resolution even with the fast phase ignored, see, e.g., [1, 3, 5, 75, 86]. For the case of extended scatterers, however, the fast phase in formula (2.31) should be retained. Keeping the fast phase is also important for SAR interferometry [111].

The fast phase term $e^{i\Phi_0}$ in (2.97) allows one to separate the scales of variation in both the imaged quantity ν and the image I into fast (on the order of wavelength) and slow (much longer than the wavelength, on the order of resolution), see Section 7.2 of Chapter 7. This, in turn, enables the backscattering via the resonant Bragg mechanism and yields a physical interpretation of the observable quantity in SAR imaging as a slowly varying amplitude of the Bragg harmonic in the spectrum of ground reflectivity. Otherwise, consider, for example, a constant refractive index, $n(\boldsymbol{z}) = \text{const}$, on a semi-space. The reflection from such a target is specular and involves no backscattering. Yet if the reflectivity $\nu(\boldsymbol{z})$ given by (2.15′) for $n(\boldsymbol{z}) = \text{const}$ is substituted into (2.31), and the fast phase term $e^{i\Phi_0}$ is not included into $W(\boldsymbol{y}, \boldsymbol{z})$, then there will be a nonzero image intensity. This leads to an inconsistency because formula (2.31) describes the monostatic SAR imaging and therefore can generate an image only if a certain part of the incident field is scattered back to the antenna.

Moreover, the intensity of the image (2.31) for a homogeneous half-space will not depend on polarization because the entire previous development is done in the scalar framework. In reality, however, the polarization needs to be taken into account. This is done in Section 7.5 of Chapter 7.

Another inconsistency in the traditional exposition of the SAR ambiguity theory is related to the representation of the ground reflectivity function in the form of a single layer on the surface of the target, see (2.93). Such a representation is usually justified by the rapid decay of the radar signal as it penetrates below the Earth's surface. From the standpoint of physics, this is an adequate consideration because the typical SAR carrier frequencies are in the microwave range and their penetration depth is small.[8] It suggests, however, that the scattering is strong, as it prevents the incident field from penetrating deep into the target. Hence, the condition for applicability of the first Born approximation, which assumes weak scattering, is violated. Moreover, a singular expression for ν in (2.93) is an obvious violation of (2.7).

We postpone the remedying of these inconsistencies until Chapter 7, i.e., until after the discussion on transionospheric SAR imaging. In Chapter 7, we address the foregoing concerns by introducing a new approach to the treatment of radar targets that will allow us to compute the scattered signal in any given direction. The new approach is more comprehensive than the previous one as it carries no constraint that the scattering has to be weak, and does not rely on the first Born approximation. Yet it keeps the inverse scattering problem for SAR linear, and eventually allows one to obtain its solution in the form of convolution (2.31), where the integral is taken only along the surface of the target. When the scattering is weak, the results obtained in the new framework become equivalent to those obtained by means of the conventional approach.

[8]The penetration depth for an electromagnetic wave can often be estimated as one half of the wavelength, see, e.g., [19, Chapter 7].

2.8 Chapter summary

We presented a traditional exposition of the SAR ambiguity theory for the case of monostatic broadside non-interferometric (i.e., 2D) imaging. Our discussion covered the interrogating waveforms (linear chirps), as well as their propagation and scattering in Section 2.1, including the first Born approximation in Section 2.1.1; the analysis of the antenna radiation pattern in Section 2.2; and that of the two-stage inversion of the raw data in Section 2.3. The two stages of inversion are the application of the matched filter (2.23), (2.24) in Section 2.3.1 (see also Appendix 2.A) and the summation over the synthetic aperture (2.31), see Section 2.3.2. In Section 2.4, we computed the imaging kernel, i.e., the GAF, and in the subsequent Section 2.5 we estimated the error associated with its factorized representation; the latter being a very convenient tool for the resolution analysis presented in Section 2.6. In Section 2.7, we outlined some inconsistencies of the traditional approach related to the use of the first Born approximation and to the absence of the resonant Bragg scale in the scattering model. These inconsistencies will be addressed in Chapter 7, i.e., after the forthcoming ionospheric discussion in Chapters 3, 4, and 5.

The most important concepts and equations in this chapter include:

- The list of assumptions right before Section 2.1;
- The retarded potential formula (2.4) for the propagation of a radar pulse in vacuum;
- The convolution formula (2.14″) for the field scattered off the target;
- Formula (2.23) for the matched filter;
- Equation (2.32) for the imaging kernel;
- The concept of factorization of the GAF represented by formula (2.77);
- Formula (2.92) for the factorization error;
- Formulae (2.95) and (2.96) that define the range and azimuthal factors of the GAF and introduce the expressions for the range and azimuthal resolution.

Appendix 2.A Choosing the matched filter

Let the received field be given by the integral [cf. formula (2.14″)]

$$u(t, \boldsymbol{x}) = \int \nu(\boldsymbol{z}) P\,(t - 2R_z/c)\, d\boldsymbol{z}, \tag{2.98}$$

where $\nu(\boldsymbol{z})$ incorporates both the ground reflectivity and the propagation attenuation, see (2.15′), and let the image be defined with the help of the function $K = K(t, \boldsymbol{y})$ [cf. formula (2.24)]:

$$I_x(\boldsymbol{y}) = \int_{-\infty}^{\infty} K(t, \boldsymbol{y}) u(t, \boldsymbol{x}) dt. \tag{2.99}$$

Substituting (2.98) into (2.99) and changing the order of integration, we arrive at a mapping $v(\boldsymbol{z}) \mapsto I_x(\boldsymbol{y})$, which is known as the imaging operator:

$$I_x(\boldsymbol{y}) = \int v(\boldsymbol{z}) \int_{-\infty}^{\infty} K(t, \boldsymbol{y}) P\left(t - 2R_z/c\right) dt d\boldsymbol{z}. \tag{2.100}$$

The function $K(t, \boldsymbol{y})$, which is at our disposal, can be chosen to achieve some desirable properties of the imaging operator (2.100).

One of those properties may be to maximize the return from isolated point scatterers. Namely, let $v(\boldsymbol{z}) = v_{z_0}\delta(\boldsymbol{z} - \boldsymbol{z}_0)$, where v_{z_0} is a constant factor and $\boldsymbol{z}_0$ is given. Then, formula (2.100) yields:

$$I_x(\boldsymbol{y}) = v_{z_0} \int_{-\infty}^{\infty} K(t, \boldsymbol{y}) P\left(t - 2R_{z_0}/c\right) dt. \tag{2.101}$$

Assume that the function $K(t, \boldsymbol{y})$ is absolutely square integrable with respect to t uniformly in $\boldsymbol{y}$, i.e., $\forall \boldsymbol{y} : \; K(t, \boldsymbol{y}) \in L_2(-\infty, \infty)$, and the estimate

$$\int_{-\infty}^{\infty} |K(t, \boldsymbol{y})|^2 \, dt \leqslant E_K \tag{2.102}$$

holds with one and the same constant E_K for all $\boldsymbol{y}$. Consider the image (2.101) at $\boldsymbol{y} = \boldsymbol{z}_0$. We will seek $K(t, \boldsymbol{y})$ that maximizes the return $I_x(\boldsymbol{z}_0)$ relative to the input v_{z_0}, i.e., maximizes the ratio $\frac{|I_x(z_0)|}{|v_{z_0}|}$, subject to constraint (2.102).

From the Cauchy-Schwarz inequality we get the following estimate:

$$|I_x(\boldsymbol{y})| = \left| v_{z_0} \int_{-\infty}^{\infty} K(t, \boldsymbol{y}) P\left(t - 2R_{z_0}/c\right) \, dt \right| \leqslant |v_{z_0}| \sqrt{E_K E_P}, \tag{2.103}$$

where

$$E_P = \int_{-\infty}^{\infty} |P(t)|^2 \, dt < \infty.$$

For the chirp (2.10), (2.11), $E_P = \tau$. The equality in (2.103) is reached only for

$$K(t, \boldsymbol{y}) = \sqrt{\frac{E_K}{E_P}} \overline{P\left(t - 2R_y/c\right)}. \tag{2.104}$$

Formula (2.104) defines the matched filter: the kernel in the integral operator (2.99) is a scaled delayed complex conjugate replica of the original signal. Moreover, it is easy to see that the resulting maximum value of $\frac{|I_x(z_0)|}{|v_{z_0}|}$ appears independent of $\boldsymbol{z}_0$. If we take $E_K = \tau$, then formula (2.104) reduces to the expression (2.23) for the matched filter that we introduced in Section 2.3.1.

The consideration based solely on point scatterers is deficient though in that the real radar targets may have a different composition. As such, instead of maximizing the return from point scatterers we may require that the kernel of the imaging operator (2.100), i.e., the PSF

$$W_{\boldsymbol{x}}(\boldsymbol{y},\boldsymbol{z}) = \int_{-\infty}^{\infty} K(t,\boldsymbol{y}) P\left(t - 2R_z/c\right)\, dt, \tag{2.105}$$

be close to the delta-function $\delta(\boldsymbol{y}-\boldsymbol{z})$. This requirement is more general than the previous one because in the case of a true equality: $W_{\boldsymbol{x}}(\boldsymbol{y},\boldsymbol{z}) = \delta(\boldsymbol{y}-\boldsymbol{z})$, the image $I(\boldsymbol{y})$ on the left-hand side of (2.100) exactly reconstructs the unknown function $\nu(\boldsymbol{z})$ regardless of its actual form.

Yet the question of how one shall understand the "closeness" between $W_{\boldsymbol{x}}(\boldsymbol{y},z)$ and $\delta(\boldsymbol{y}-\boldsymbol{z})$ requires attention, because spaces of distributions are not equipped with norms. We will use the spectral interpretation, i.e., employ the Fourier transform. Namely, let $\tilde{K}$ and $\tilde{P}$ denote the Fourier transforms of K and P, respectively, in time:

$$\tilde{K}(\omega,\boldsymbol{y}) = \int_{\infty}^{\infty} K(t,\boldsymbol{y}) e^{i\omega t} dt, \quad \tilde{P}(\omega) = \int_{\infty}^{\infty} P(t) e^{i\omega t} dt.$$

Then, taking into account that the Fourier transform of a product is the convolution of Fourier transforms, for the PSF (2.105) we can write:

$$W_{\boldsymbol{x}}(\boldsymbol{y},\boldsymbol{z}) = \frac{1}{2\pi} \int_{-\infty}^{\infty} e^{i\omega 2R_z/c} \tilde{P}(\omega) \tilde{K}(-\omega,\boldsymbol{y})\, d\omega. \tag{2.106}$$

For the rest of this section, we will adopt a simplified one-dimensional setting, for which $\boldsymbol{y} = R_y \equiv y$ and $\boldsymbol{z} = R_z \equiv z$. Then, the following identity holds:

$$\delta(y-z) = \frac{2}{c}\delta\left(2R_y/c - 2R_z/c\right) = \frac{2}{c}\frac{1}{2\pi}\int_{-\infty}^{\infty} e^{-i\omega 2(R_y-R_z)/c} d\omega.$$

Matching the right-hand side of the previous equality against that of (2.106), we see that if

$$\tilde{P}(\omega)\tilde{K}(-\omega,y) = e^{-i\omega 2R_y/c}, \tag{2.107}$$

then the spectra of the two expressions differ only by the constant $\frac{2}{c}$, which is not essential. Consequently, if (2.107) could be satisfied for all ω, then $W_{\boldsymbol{x}}(y,z)$ will be proportional to $\delta(y-z)$, which is our goal.

However, choosing $\tilde{K}(\omega,y)$ to satisfy (2.107) for all $\omega \in \mathbb{R}$ is not possible if $\tilde{P}(\omega)$ is zero (or very small by absolute value) for a range of frequencies. This appears to be the case for the chirped signals (2.10), (2.11) that are designed to have their spectrum confined to a band of width B around the central carrier frequency ω_0:

$$\begin{aligned} \tilde{P}(\omega) &= \int_{-\infty}^{\infty} \chi_\tau(t) e^{-i\alpha t^2} e^{-i\omega_0 t} e^{i\omega t}\, dt \\ &\approx \sqrt{\frac{\pi}{\alpha}} e^{-i\pi/4} e^{i(\omega-\omega_0)^2/(4\alpha)} \chi_B(\omega-\omega_0). \end{aligned} \tag{2.108}$$

The integration in (2.108) has been performed using the method of stationary phase, and the factor

$$\chi_B(\omega-\omega_0) \stackrel{\text{def}}{=} \begin{cases} 1, & |\omega-\omega_0| \leqslant B/2, \\ 0, & \text{otherwise}, \end{cases} \tag{2.109}$$

on the last line of (2.108) originates from the condition that the stationary point of the phase

$$t_{\text{st}} = \frac{\omega-\omega_0}{2\alpha} \tag{2.110}$$

must belong to the interval $[-\tau/2, \tau/2]$ defined by the indicator function $\chi_\tau(t)$ of (2.11).[9] It is only in the frequency band $|\omega-\omega_0| \leqslant B/2$ defined by (2.109) that $\tilde{K}(\omega, y)$ can be chosen to satisfy (2.107):

$$\tilde{K}(\omega, y) = \frac{1}{\tilde{P}(-\omega)} e^{i\omega 2R_y/c} = \text{const} \cdot \tilde{\overline{P}}(\omega) e^{i\omega 2R_y/c}, \tag{2.111}$$

where $\tilde{\overline{P}}(\omega)$ denotes the Fourier transform of the complex conjugate of $P(t)$, and the second equality in (2.111) is derived with the help of (2.108) and (2.109). Applying the inverse Fourier transform to (2.111), we obtain:

$$K(t, y) \propto \overline{P(t-2R_y/c)}, \tag{2.112}$$

which coincides with the matched filter expression (2.104). Hence, for the chirped signals the matched filter formula (2.104) also satisfies (2.107) so that the spectrum of $W_{\boldsymbol{x}}(y, z) = W_{\boldsymbol{x}}(y-z)$ coincides with that of $\delta(y-z)$ for $|\omega-\omega_0| \leqslant B/2$. In this sense, $W_{\boldsymbol{x}}(y-z)$ can be considered an approximation to $\delta(y-z)$.

[9] The method of stationary phase provides only an approximate, rather than exact, value of the Fourier integral in (2.108). Therefore, the actual spectrum of the chirp (2.10), (2.11) extends beyond the interval $\omega \in [\omega_0 - B/2, \omega_0 + B/2]$. Its more accurate computation would require the analysis of the case where the stationary point (2.110) is located at or near either of the endpoints of the integration interval $t \in [-\tau/2, \tau/2]$, including the situation when it is outside of this interval, see, e.g., [112, Chapter III, Section 1] for detail. The exact spectrum of the chirp can be expressed via the erf(·) functions of a complex argument, see, e.g., [5], although for obtaining practical estimates the resulting expressions still need to be approximated.

http://www.springer.com/978-3-319-52125-1

Transionospheric Synthetic Aperture Imaging

Gilman, M.; Smith, E.; Tsynkov, S.

2017, XXIII, 458 p. 25 illus., 16 illus. in color., Hardcover
ISBN: 978-3-319-52125-1
A product of Birkhäuser Basel